# Whole body metabolism, muscle and mitochondrial function, and the role of uncoupling protein-3 in a mouse model of sepsis.

Dr Parjam Seyed Zolfaghari

A thesis submitted for the Degree of Doctor of Philosophy

University College London

Funded by the Medical Research Council

2012

## DECLARATION

I, Parjam Seyed Zolfaghari confirm that the work presented in this thesis is my own. Where information has been derived from other sources, I confirm that this has been indicated in the thesis.

## ABSTRACT

Sepsis, the exaggerated systemic inflammatory response to infection, often leads to multi-organ failure (MOF) and death. Skeletal muscle function is often profoundly affected, with patients requiring prolonged ventilatory support and rehabilitation. The pathophysiology underlying MOF and muscle failure in sepsis remains poorly understood. Recent evidence points to mitochondrial dysfunction and cellular energetic down-regulation, related in part to excess generation of reactive oxygen and nitrogen species (ROS). Substrate oxidation by the mitochondrial respiratory chain generates a proton gradient across the inner mitochondrial membrane that is coupled to ATP production. Mitochondrial uncoupling proteins (UCPs) may reduce mitochondrial ROS formation, though at the expense of oxidative phsophorylation. Notably, UCP3 is up-regulated in sepsis but its physiological role is unknown. I therefore hypothesized that muscle dysfunction in sepsis has a mitochondrial aetiology and increased UCP3 expression offers a protective role. I investigated this in a fluid-resuscitated murine model of faecal peritonitis/MOF (optimized and characterized during this project). I used *Ucp3*$^{(-/-)}$ mice to explore the role of this uncoupling protein in sepsis.

I observed a profound hypothermic and hypometabolic response early in the course of severe sepsis. This was accompanied by respiratory muscle dysfunction and fatigue, as well as a decrease in mitochondrial proton-motive force (measured using novel live-cell 2-photon confocal imaging techniques in freshly isolated *ex-vivo* diaphragm muscles). By contrast, the mitochondrial proton-motive force was

unaffected in septic *Ucp3*$^{(-/-)}$ mice, but no difference was seen in whole-body metabolic response or respiratory muscle fatigue. Furthermore, proton leak and substrate utilization of mitochondria isolated from whole body skeletal muscle from wild-type septic mice were unchanged, though superoxide production was higher. These findings suggest that up-regulation of UCP3 in sepsis has no whole- body metabolic or functional consequence in skeletal muscle. The low global oxygen consumption and diaphragm mitochondrial proton-motive force suggest a reduced cellular metabolic demand in the septic mice.

## ACKNOWLEDGMENTS

I would like to extend my gratitude to my supervisors Professors Mervyn Singer (UCL), Michael Duchen (UCL) and Nancy Curtin (Imperial college), for their energy, guidance and advice throughout this project. Also to Drs Jane Carre, Nadeene Parker, Sean Davidson and Alex Dyson for their invaluable help with technical and theoretical aspects of the project as well as guidance in preparation of this manuscript.

A special thanks also to Valerie Taylor and Raymond Stidwill for teaching and assistance with animal husbandry, surgery and *in vivo* experiments.

This project was kindly funded by the Medical Research Council through a Clinical Research Training Fellowship.

I would like to thank my wife, Dr Louise Barber, for help and support at home, and frequent trouble-shooting with science, computers and software! Also for bringing to life our daughter Ayla who has brought joy and perspective to our lives.

Finally, I would like to dedicate this body of work to the memory of my father, Seyed Abbas Zolfaghari, who is missed greatly and forever in our hearts.

## TABLE OF CONTENTS

## LIST OF FIGURES

## LIST OF TABLES

# Abbreviations

| | |
|---|---|
| $\Delta\psi_m$ | Mitochondrial membrane potential |
| ADP | Adenosine diphosphate |
| ALT | Alanine transferase |
| AM | Acetoxymethyl ester group |
| AMP | Adenosine monophosphate |
| ANOVA | Analysis of variance |
| ANT | Adenine nucleotide translocase |
| AST | Aspartate transaminase |
| ATP | Adenosine triphosphate |
| BSA | Bovine serum albumin |
| BE | Base excess |
| $[Ca^{2+}]_c$ | Cytosolic calcium concentration |
| $[Ca^{2+}]_m$ | Mitochondrial calcium concentration |
| $[Ca^{2+}]_I$ | Intracellular calcium concentration |
| CIPNM | Critical illness polyneuropathy and myopathy |
| CLP | Caecal ligation and puncture |
| $CN^-$ | Cyanide |
| Cr | Creatine |
| CSA | Cross-sectional area |
| CS | Citrate synthase |
| DHE | Dihydroethidine |
| DTNB | 5, 5` dithio-bis (2-nitrobenzoic acid) () |
| DNP | 2,4-dinitrophenol |
| dNTP | Deoxyribonucleotide triphosphate |
| EDD | End-diastolic diameter |
| EDTA | Ethylenediaminetetraacetic acid |
| ESD | End-systolic diameter |
| $FADH_2$ | Flavin adenine dinucleotide ($FAD^{2+}$ oxidized form) |
| FCCP | Carbonyl-cyanide-p-trifluoromethoxyphenyl hydrazone |
| GA | General anaesthesia |
| GDP | Guanosine diphosphate |

| | |
|---|---|
| GFP | Green fluorescent protein |
| Hb | Haemoglobin concentration |
| HIF-1α | Hypoxia inducible factor 1α |
| HNE | Hydroxynonenal |
| HRP | Horse-radish peroxidase |
| $H_2O_2$ | Hydrogen peroxide |
| iNOS | Inducible isoform of nitric oxide synthase |
| INS-1 | Insulinoma cell line |
| i/p | Intraperitoneal |
| i/v | Intravenous |
| $K_{ATP}$ | ATP dependent potassium channel |
| $L_0$ | Muscle length with optimal tetanic force development |
| $L_W$ | Muscle length for optimal work and power output |
| LPS | Lipopolysaccharide |
| LV | Left ventricle |
| MAC | Minimum alveolar concentration |
| MDMA | 3,4-methylenedioxymethylamphetamine |
| MitoQ | Mitochondrial targeted anti-oxidant |
| MOF | Multiorgan failure |
| MODS | Multiorgan dysfunction syndrome |
| mPTP | Membrane permeability transition pore |
| NADH | Nicotinamide adenine dinucleotide ($NAD^+$ oxidized form) |
| NO | Nitric oxide |
| $O_2^{\cdot-}$ | Superoxide |
| $ONOO^-$ | Peroxynitrite |
| OW | One-way |
| PCr | Phosphocreatine |
| PCR | Polymerase chain reaction |
| PDK | Pyruvate dehydrogenase kinase |
| PDC | Pyruvate decarboxylase |
| PEG-SOD | Pegylated superoxide dismutase and |
| Pi | Inorganic phosphate |
| PV | Peak velocity |
| RCR | Respiratory control ratio |

| | |
|---|---|
| RER | Respiratory exchange ratio |
| RM-ANOVA | Repeated measures ANOVA |
| $RNOO^-$ | Peroxynitrite |
| RNS | Reactive nitrogen species |
| ROS | Reactive oxygen species |
| RV | Right ventricle |
| s/c | Subcutaneous |
| SD | Standard deviation |
| SDS | Sodium dodecyl sulphate |
| SEM | Standard error of mean |
| SERCA | Sarco-endoplasmic reticulum $Ca^{2+}$ ATPase |
| SIRS | Systemic inflammatory response syndrome |
| SOFA | Sequential organ failure assessment |
| SR | Sarcoplasmic reticulum (SR) |
| SOD | Superoxide dismutase |
| SV | Stroke volume |
| TCA | Tricarboxylic acid |
| TAE | Tris base, acetic acid and EDTA |
| TMRM | Tetramethylrhodamine methyl ester |
| TNB | Thionitrobenzoic acid |
| $TPMP^+$ | Methyltriphenylphosphonium |
| $tPO_2$ | Partial pressure of tissue oxygen |
| TW | Two-way |
| UCP1/2/3 | Uncoupling proteins-1, 2, 3 |
| $VCO_2$ | Whole body $CO_2$ production |
| $VO_2$ | Whole body oxygen consumption |
| VTI | Velocity time integral |
| WT | Wild-type |

# CHAPTER 1. INTRODUCTION

## 1.1 Sepsis definition and epidemiology

The Systemic Inflammatory Response Syndrome (SIRS) is the result of an exaggerated whole body response to an exogenous insult such as trauma, ischaemia/reperfusion or toxins. When infection is the underlying aetiology it is termed *sepsis* (Bone, Balk et al. 1992). SIRS is defined by the presence of at least two of the following:

1. Body temperature >38°C or <36°C
2. Heart rate >90 beats/minute
3. Hyperventilation (resp. rate >20/min or $PaCO_2$ of <4.25 kPa)
4. White blood cell count of >12,000 or <4,000 cells/litre

Following the International Sepsis Definition Conference in 2001, the above criteria were widened to include hyperglycaemia in the absence of diabetes, altered mental status, hyperlactataemia and decreased capillary refill (Levy, Fink et al. 2003). *Severe sepsis* is associated with organ dysfunction whereas *septic shock* is severe sepsis associated with persisting hypotension despite appropriate volume resuscitation.

Sepsis carries a high mortality and morbidity. Of 343,860 UK intensive care unit admissions from 1996-2004, 27% fufilled severe sepsis criteria within 24 h of admission and their mortality rate was 45% (Harrison, Welch et al. 2006). The incidence of sepsis in the US was reported to be 153 cases per 100,000 with a hospital mortality rate of 28.5% and an associated cost of $22,100 per case (Angus, Linde-Zwirble

et al. 2001). Another US study showed a three-fold increase in incidence over two decades (Martin, Mannino et al. 2003). Despite medical advances, up to 50% of patients still die as a result of severe sepsis (Vincent, Abraham et al. 2002). Although the demographic is changing with more elderly and immunosuppressed patients being treated, our incomplete appreciation of the underlying mechanisms of the disease is also a major contributor to our relative lack of progress.

### 1.2 The pathophysiology of sepsis and multi-organ failure

Inflammatory-immune changes occurring during sepsis are both complex and time-dependent (reviewed by (Hotchkiss and Karl 2003)). While the early phase is characterized by an increase in pro-inflammatory mediators (a “cytokine storm”) with increased production of reactive oxygen (ROS) and nitrogen species (RNS) (Biswal and Remick 2007), this is replaced within hours to days by an overall immunosuppressive phenotype and an increased susceptibility to nosocomial infection (Osuchowski, Welch et al. 2006; Monneret, Venet et al. 2008; Hotchkiss, Coopersmith et al. 2009). Immune cells show reduced responsiveness to antigen (Ward, Casserly et al. 2008; Adib-Conquy and Cavaillon 2009) while apoptosis is increased in lymphocytes but delayed in neutrophils (Hotchkiss, Swanson et al. 1999).

Concurrent changes are seen in macro- and microcirculatory function, in activation of coagulation and fibrinolytic pathways, and in hormonal, bioenergetic and metabolic pathways. Remarkably, apart from an influx of inflammatory cells and increased tissue oedema, there is little

structural damage to affected organs with minimal cell death (Hotchkiss, Swanson et al. 1999). In a systematic review of histopathological changes found in patients and animals with septic acute kidney injury, acute tubular necrosis was a rare event (Langenberg, Bagshaw et al. 2008). Notably, organ dysfunction tends to recover within days-to-weeks in survivors, even in organs that are generally poorly regenerative such as the kidney (Noble, MacKirdy et al. 2001; Bagshaw, Uchino et al. 2007). It has been postulated that the organism enters into a state of "cellular energy dormancy" as an evolutionary adaptation to enhance the likelihood of survival from an otherwise overwhelming external insult (Singer, De Santis et al. 2004).

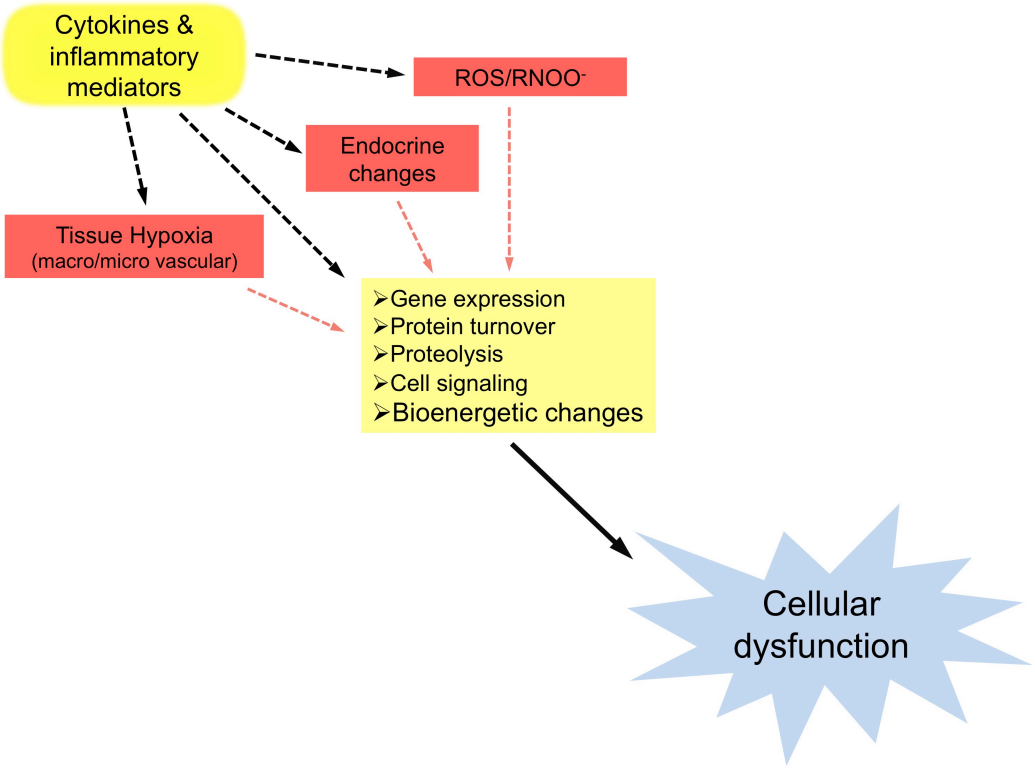


**Figure 1.1** Simplified diagram of proposed mechanisms of cellular dysfunction in sepsis. Although the arrows point in one direction, in reality the processes identified above are likely to be more interdependent.

### 1.2.1 Tissue $pO_2$ in septic multi-organ failure

Patients with severe sepsis often present with lactataemia and metabolic acidosis suggestive of poor tissue perfusion (De Backer 2003; Dellinger, Levy et al. 2008). However, direct measurements of tissue $pO_2$ ($tPo_2$) in skeletal muscle of septic patients (Boekstegers, Weidenhöfer et al. 1994), and in gut (VanderMeer, Wang et al. 1995) and bladder epithelium (Rosser, Stidwill et al. 1995) in animal models reported elevated levels of $tPo_2$. As $tPo_2$ represents the dynamic equilibrium between local supply and utilization of oxygen, this suggests a relative availability but non-utilization of oxygen. Importantly, these data challenge traditionally held view that multi-organ failure in sepsis is simply due to tissue hypoxia (Protti and Singer 2006).

Other data support this hypothesis. For example, peripheral limb oxygen consumption measured during a short-lived vascular occlusion was reduced in septic patients compared to age-matched healthy volunteers or patients with localized infection (De Blasi, Palmisani et al. 2005; Pareznik, Knezevic et al. 2006). This correlated with sepsis severity but improved as the patients recovered. Recovery on restoration of blood flow was also impaired, suggesting a concurrent problem with tissue flow and vascular recruitment (Payen, Luengo et al. 2009).

My host lab recently reported changes in $tPo_2$ from peripheral (skeletal muscle and bladder epithelium) and central (kidney and liver) organs in a long-term fluid-resuscitated model of faecal peritonitis (Dyson, Bezemer et al. 2011). Early (6 hour) falls in muscle, renal and hepatic $tPo_2$ were followed by normalization at 24h, despite worsening clinical

and biochemical status including hyperlactataemia. Indeed, the significance of serum lactate levels as a marker of global tissue hypoxia and anaerobic respiration in sepsis has been questioned (James, Luchette et al. 1999). High lactate levels can occur as a result of accelerated aerobic glycolysis coupled to skeletal muscle $Na^+/K^+$ ATPase activity stimulated by high levels of endogenous epinephrine in septic shock (Levy, Gibot et al. 2005).

The role of tissue hypoxia in amplifying the systemic inflammatory response should not however be discounted as early haemodynamic interventions to correct tissue perfusion resulted in significantly reduced mortality (Rivers, Nguyen et al. 2001). Later attempts at correction, once the patient was already in established organ failure, offered either no benefit (Gattinoni, Brazzi et al. 1995) or even harm (Hayes, Timmins et al. 1994). Tissue hypoxia in itself may trigger a shutdown of cellular metabolism that synergizes with direct inhibition (or damage) of mitochondrial respiration (Frost, Wang et al. 2005). This may explain why sepsis-induced changes in cellular metabolism may not be promptly reversible (Kern and Shoemaker 2002; Poeze, Greve et al. 2005).

### 1.2.2 Whole body metabolism and temperature in sepsis

The data presented above suggest reduced cellular metabolism in sepsis. In terms of whole body metabolism, patients with sepsis and septic shock show an average 10-15% increase in resting energy expenditure compared to healthy, age-matched normal subjects

(Chioléro, Revelly et al. 1997; Miles 2006). Values are approximately twice normal in uncomplicated sepsis fall to normal values in septic shock but rise significantly during recovery (61±22% above normal) (Kreymann, Grosser et al. 1993). Similar findings have been reported in neonatal and paediatric sepsis where a predominantly hypometabolic response was observed in those with septic shock and multi-organ failure (Briassoulis, Venkataraman et al. 2010; Feferbaum, Leone et al. 2010). The hypermetabolic pattern only emerged during the recovery phase.

Importantly, core body temperature changes of 1ºC results in 10% changes in $VO_2$ (Manthous, Hall et al. 1995; Bruder, Raynal et al. 1998). Ten percent of adult septic patients present with hypothermia and this is independently associated with a two-fold increase in mortality (Clemmer, Fisher et al. 1992; Arons, Wheeler et al. 1999). Cellular metabolism of such patients will likely be significantly lower, although Kreymann *et al* (Kreymann, Grosser et al. 1993) could find no correlation between $VO_2$ and temperature. This hints at a more complex relationship between temperature and $VO_2$ in sepsis.

Animal studies confirm hypothermic and hypometabolic responses in young animals (Garrett-Cox, Pierro et al. 2003). However, adult rats injected with intraperitoneal endotoxin (LPS) show variable temperature responses depending on the dose and type of LPS injected (Dogan, Ataoglu et al. 2000). In general, a biphasic pattern of early hypothermia followed by normothermia or pyrexia is observed. The extent of the initial hypothermia is dose-dependent and associated with falls in blood pressure (Romanovsky, Shido et al. 1996; Dogan, Ataoglu et al. 2000).

Mice however exhibit an opposite pattern when challenged with LPS. Following an early rise in temperature, they become hypothermic depending on LPS dose, ambient temperature and the degree of stress suffered (Leon 2004; Rudaya, Steiner et al. 2005).

Caecal ligation and puncture (CLP) in mice is associated with hypothermia, reductions in $VO_2$ and a fall in respiratory exchange ratio from 0.85 to 0.7, favouring lipid metabolism (Valencia, Sarma et al. 2005). The severity of these changes were not predictive of survival. In another study, intra-peritoneal implantation of fibrin clot inoculated with *Staphylococcus aureus* in mice resulted in a one-third reduction in $VO_2$ (Haden, Suliman et al. 2007); clinical recovery occurred within 3-7 days and was preceded by mitochondrial biogenesis (discussed later).

The hypothermic response in septic animal models was originally thought to be circulatory in origin. However, this appears to be a regulated response affected by ambient temperature and the degree of stress placed on the animal (reviewed by (Leon 2004)). This may offer survival benefits (Habicht 1981; Romanovsky, Shido et al. 1997). Pyrexia and hypothermia may thus be two distinct strategies of fighting systemic inflammation offering benefit under differing conditions (Romanovsky and Székely 1998). Fever may support host defence mechanisms against the invading organism, whereas hypothermia may act as a defensive mechanism that support the host's vital functions by reducing metabolic demands.

## 1.3 Mitochondrial physiology and sepsis

Mitochondria utilise >90% of the body's total oxygen consumption. This is predominantly for generating adenosine 5'-triphosphate (ATP), the crucial energy currency for cellular processes. The host lab has shown in septic patients, animal models and *in vitro* models that mitochondrial dysfunction is closely associated with multi-organ failure (Brealey, Brand et al. 2002; Brealey, Karyampudi et al. 2004; Frost, Wang et al. 2005). Patients who eventually died had significantly lower muscle ATP levels (Brealey, Brand et al. 2002), a finding replicated in liver and muscle in a 3-day rodent faecal peritonitis model (Brealey, Karyampudi et al. 2004). Inhibition of mitochondrial respiration by increased production of nitric oxide and its derivative peroxynitrite is implicated in the causation of this bioenergetic failure (Brown and Borutaite 2004; Frost, Wang et al. 2005) .

### 1.3.1 Cellular and mitochondrial metabolism

Mitochondrial ATP production begins with cytosolic metabolism of high-energy glucose and fatty acid molecules. Glycolysis results in the net production of 2 ATP molecules per glucose molecule, and the formation of pyruvate which is taken up and metabolized within mitochondria to produce a further 30 or so ATP molecules. Pyruvate and fatty acyl CoA enter the citric acid cycle and generate the high energy reduced co-enzymes, nicotinamide adenine dinucleotide (NADH) and flavin adenine dinucleotide ($FADH_2$). These molecules act as reducing equivalents that donate electrons to the electron transport chain. As the

electrons pass down the chain, energy is captured in the form of a proton gradient which is then utilised to generate ATP (Fig 1.2).

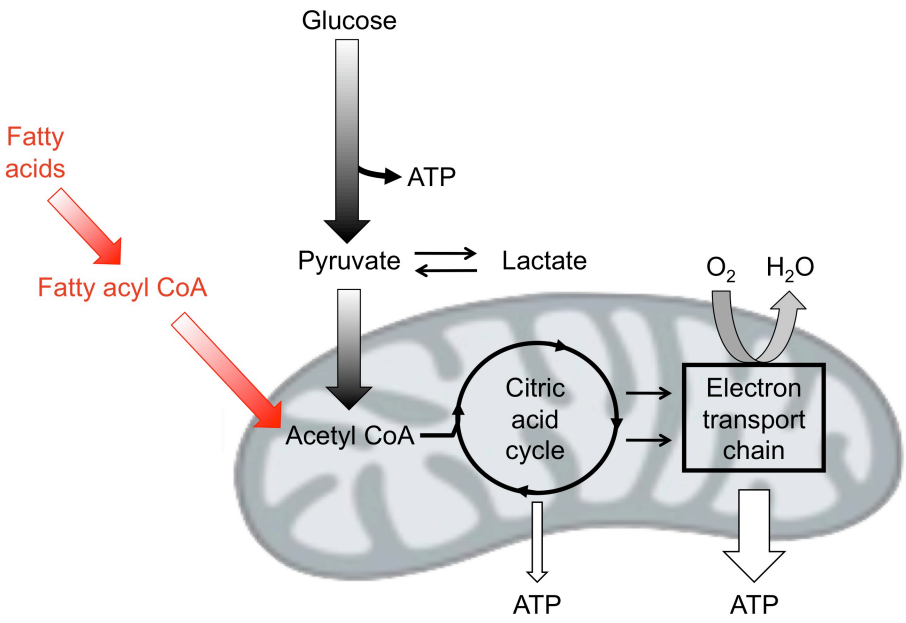


**Figure 1.2** Glycolysis and lipolysis provide substrate to the citric acid (Krebs') cycle. Through NADH and FAD, electrons are donated to the electron transport chain resulting in significantly larger production of ATP.

### 1.3.1.1 The electron transport chain and ATP synthesis

The electron transport chain is composed of five enzyme complexes held within the inner mitochondrial membrane. Compared with the highly porous outer membrane, the inner membrane is tightly bound with transporter molecules shuttling molecules and solutes across the membrane (Fig 1.3). The first four respiratory chain complexes are involved in substrate oxidation and formation of an energy gradient, while

the fifth (ATP synthase) utilises this gradient to generate ATP.

NADH and $FADH_2$ produced by the Krebs' cycle donate electrons to complexes I (NADH dehydrogenase) and II (succinate dehydrogenase), respectively. Oxidized NAD+ and FAD then re-enter the cycle. Donated electrons are passed to complexes III (cytochrome $bc_1$) and IV (cytochrome c oxidase) where molecular oxygen acts as the terminal oxygen acceptor. During this process, protons are pumped out of the mitochondrial matrix into the intermembrane space by complexes I, III and IV, generating a proton gradient across the membrane. This charge difference, the mitochondrial transmembrane potential ($\Delta\psi_m$), normally rests at -150 to -180mV (Fig. 1.3). It serves as a store of energy for the various energetic processes that take place across the inner membrane (e.g. ATP production and various transport processes).

In isolation, complex V (the $F_1F_0$-ATP synthase) acts as an ATPase, breaking down ATP to transport protons out of the mitochondrial matrix. However, when *in situ* within the charged inner membrane of the mitochondria, it works in reverse, driven by the energy stored in the form of the $\Delta\psi_m$ to generate ATP (Nicholls and Ferguson 2002). ATP production by complex V therefore depends upon the magnitude of $\Delta\psi_m$ and the ability of the respiratory chain to maintain $\Delta\psi_m$ (Fig 1.4). This was the basis of the chemiosmotic theory developed by Peter Mitchell in 1961 for which he received the Nobel prize (MITCHELL 1961).

Under ischaemic/anoxic conditions, the respiratory chain cannot maintain the protonmotive force. The resultant thermodynamic conditions

favour reverse function of the ATP synthase (Jennings, Reimer et al. 1991; Nicholls and Ferguson 2002) which now switches to its native ATPase function, consuming ATP and pumping protons out of the mitochondrial matrix. This maintains $\Delta\psi_m$ at the expense of ATP depletion (reviewed by (Duchen 2004)). The rapidly falling ATP levels lead to energy depletion within the cell, however the maintained $\Delta\psi_m$ means that mitochondrial integrity is retained, as mitochondrial depolarisation may be a trigger for apoptosis.

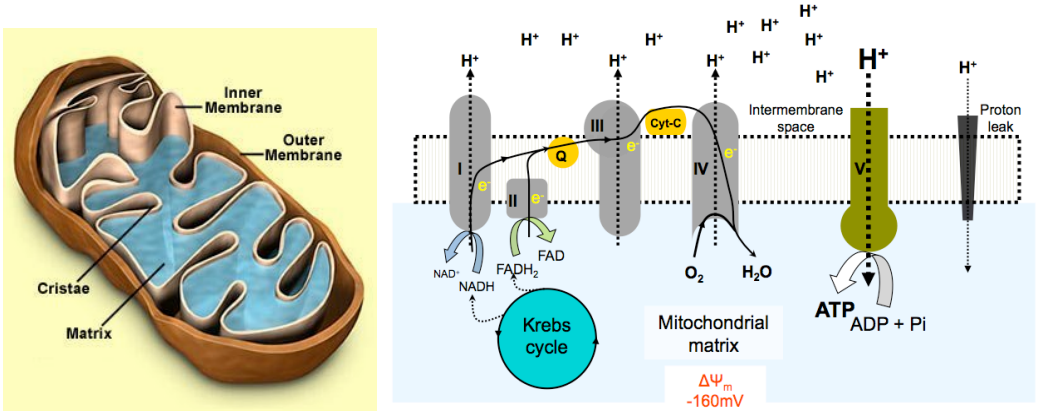


**Figure 1.3** Diagram showing the internal structure of mitochondria (left panel) with the convoluted inner mitochondrial membrane housing the respiratory chain (right panel). The first four complexes of the respiratory chain are involved in substrate oxidation with reduction of oxygen to water. Protons pumped out of the mitochondrial matrix during this process generate a proton gradient (transmembrane potential-$\Delta\psi_m$) used by complex V (ATP synthase) to produce ATP. Some protons leak directly back into the mitochondrial matrix, either passively or through specialized proteins (uncoupling proteins), bypassing ATP synthesis.

#### 1.3.1.2 Mitochondrial proton leak

The mitochondrial protonmotive force ($\Delta\psi_m$) is mainly used to convert ADP to ATP. This process of coupled oxidative phosphorylation is incomplete as some protons leak back into the mitochondrial matrix bypassing ATP synthesis and generating heat instead. This "proton leak", increases in magnitude exponentially as the transmembrane potential rises. It is split into two components (reviewed by (Jastroch, Divakaruni et al. 2010)):

1. **Basal proton leak:** This constitutes ~20% of basal metabolic rate (BMR) of hepatocytes, and up to 50% in rat skeletal muscle (Noble, MacKirdy et al. 2001). It depends on the phospholipid constitution of the lipid bilayer and the abundance of anion carrier proteins, e.g. adenine nucleotide translocase (ANT) and uncoupling protein-1 (UCP-1) within the inner mitochondrial membrane. ANT is normally responsible for shuttling ATP and ADP across this membrane.

2. **Inducible proton leak:** This is mediated by activation of ANT and UCP-1 proteins by fatty acids and reactive alkenals such as hydroxynonenal (HNE). UCP-1 (also known as thermogenin) is expressed abundantly in brown fat mitochondria and is responsible for adrenergic-stimulated mitochondrial uncoupling during non-shivering thermogenesis (Nicholls 2001). UCP-1 catalyzes a regulated passage of protons back into the mitochondrial matrix but generates heat rather than capturing their energy in the form of ATP or other chemical processes. The functions of uncoupling proteins -2 and -3 are more controversial and will be discussed later.

Uncoupling of oxidative phosphorylation has been studied in obesity and diabetes. Chemical uncoupling agents such as 2,4-dinitrophenol (DNP) have been used for weight control (Harper, Dickinson et al. 2001). However, following a series of deaths and serious illnesses, this drug was withdrawn in 1938. Clearly, mitochondrial proton leak has a significant impact upon both cellular and whole animal metabolism, though its role in pathophysiological states is less clearly defined.

#### 1.3.1.3 Mitochondria and reactive oxygen species (ROS)

Mitochondria are the major source (90%) of cellular reactive oxygen species (ROS) production within the body (reviews by (Balaban, Nemoto et al. 2005) and (Murphy 2009)). At low concentrations, mitochondrial ROS serve a redox signaling role to the rest of the cell (Dröge 2002). However, at higher concentrations, these highly reactive species cause inhibition or direct damage to proteins and other cellular components. They are implicated in a variety of pathological processes including ischaemia-reperfusion injury (Li and Jackson 2002), sepsis and ageing (Balaban, Nemoto et al. 2005). ROS are produced predominantly as superoxide ($O_2^{\cdot -}$) at complexes I and III under reducing conditions when the mitochondrial matrix NADH/$NAD^+$ ratio is high, or when $\Delta\psi_m$ is high with a low flux through the respiratory chain. Conversely, when mitochondria are making ATP at high electron flux, the rate of ROS production is much lower (Votyakova and Reynolds 2001; St-Pierre, Buckingham et al. 2002). Cytoplasmic and mitochondrial superoxide dismutase convert $O_2^{\cdot -}$ to hydrogen peroxide ($H_2O_2$) that is then

deactivated by anti-oxidant mechanisms (e.g. catalase and glutathione peroxidases) that are also present in both mitochondrial matrix and cytoplasm. Figure 1.4 shows the major sites of mitochondrial ROS production.

Sepsis is associated with increased ROS production (Nethery, DiMarco et al. 1999; Zhang, Slutsky et al. 2000), depletion of intracellular anti-oxidant stores (Brealey, Brand et al. 2002; Brealey, Karyampudi et al. 2004), and increased markers of oxidative stress (Andrades, Ritter et al. 2009; Supinski, Murphy et al. 2009). ROS production in sepsis arises from both activation of leukocytes (Zhang, Slutsky et al. 2000) and from mitochondria (Llesuy, Evelson et al. 1994; Taylor, Ghio et al. 1995; Kozlov, Staniek et al. 2006; Supinski and Callahan 2006). Mitochondrially-targetted anti-oxidant treatments such as pegylated superoxide dismutase (PEG-SOD) and MitoQ have shown improvements in cellular and mitochondrial dysfunction in sepsis (Supinski and Callahan 2006; Supinski, Murphy et al. 2009), (Lowes, Thottakam et al. 2008). Non-specific anti-oxidants such as N-acetylcysteine (NAC) and desferrioxamine have also resulted in improved cellular and mitochondrial function (Zapelini, Rezin et al. 2008). Thus, low level mitochondrial ROS production serves a signaling role in health whereas excess production, as seen in sepsis, can damage mitochondria and other cellular structures.

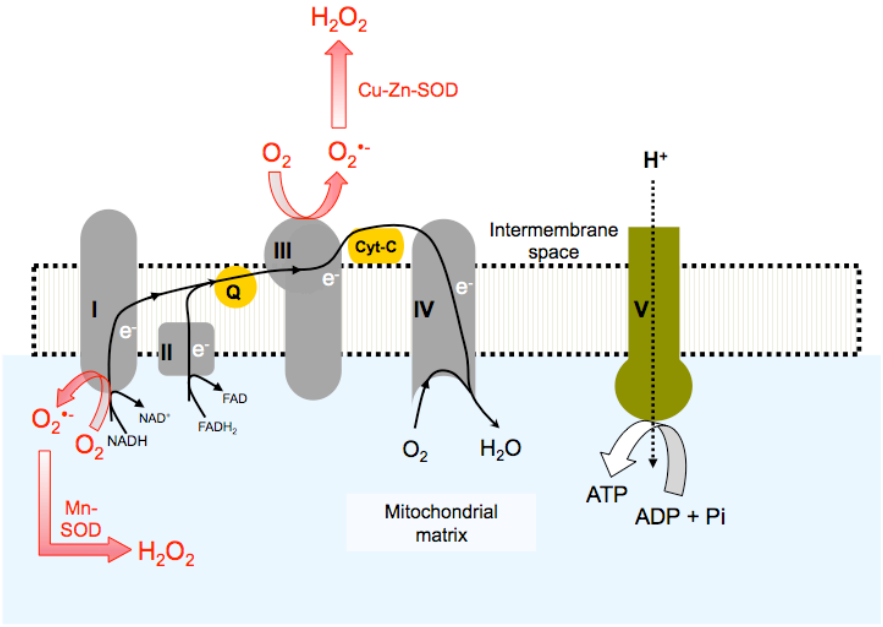


**Figure 1.4** Mitochondrial superoxide production occurs predominantly at complexes I and III. At high transmembrane potentials, when electron flux down the respiratory chain slows, the unpaired electrons more readily interact with $O_2$, resulting in increased superoxide production. Mitochondrial depolarisation has the opposite effect as electron flux increases. Superoxide dismutase (SOD) converts superoxide to $H_2O_2$. Mitochondrial and cellular anti-oxidant mechanisms such as catalase and glutathione neutralize reactive species and limit cellular damage.

### 1.3.2 Nitric oxide, sepsis and mitochondrial physiology

In sepsis, a major source of excess NO production is increased expression of the inducible isoform of nitric oxide synthase (iNOS) (Boczkowski, Lanone et al. 1996; Carreras, Franco et al. 2004). Nitric oxide (NO) reacts with $O_2$ to form $NO_2$ and $N_2O_3$, or with superoxide ($O_2^{\bullet-}$) to form peroxynitrite ($ONOO^-$) and other highly reactive nitrogen species

(RNS). These can oxidize, nitrate, nitrosate and nitrosylate amines and thiols. NO and its metabolites contribute towards vascular hyporeactivity (Levy, Collin et al. 2010), cardiac dysfunction (Rudiger and Singer 2007), skeletal muscle contractile dysfunction and mitochondrial inhibition. High nitrite and nitrate levels (metabolites of NO) are observed in human sepsis and animal models, and are associated with reduced levels of ATP and oxidative phsophorylation (Callahan, Stofan et al. 2001; Brealey, Brand et al. 2002; Brealey, Karyampudi et al. 2004).

Effects of NO on mitochondrial function include (Brown and Borutaite 2001):

1. Inhibition of the respiratory chain
2. Stimulation of reactive oxygen and nitrogen species production
3. Induction of permeability transition

NO is a potent inhibitor of cytochrome oxidase (complex IV of the respiratory chain) by competing directly with $O_2$. The reversibility of this inhibition has led to speculation that NO may regulate oxidative metabolism (Brown 2001). More prolonged exposure to NO leads to formation of other RNS, in particular $ONOO^-$, that can irreversibly inhibit respiratory chain complexes, particularly complex I. Inhibition of the respiratory chain increased production of ROS, which can further react with NO to form even more $ONOO^-$ (Poderoso, Carreras et al. 1996). This vicious spiral may eventually lead to cell dysfunction and even death. Decreased mitochondrial respiratory rates and higher ROS production have been reported in skeletal muscle of rodent models of endotoxaemia and caecal ligation/puncture (Boczkowski, Lisdero et al. 1999; Callahan,

Stofan et al. 2001).

A large multi-centre randomized controlled trial of a NOS inhibitor in sepsis was stopped early due to excess mortality in the treatment groups (López, Lorente et al. 2004). However, the NOS inhibitor used was non-selective, affecting all NOS isoforms and likely to have even blocked the adaptive consequences of increased NO synthesis (Cobb 1999; Hotchkiss, Swanson et al. 1999).

### 1.3.3 Mitochondrial calcium accumulation

Transport of large molecules and cations such as $Ca^{2+}$ across the inner mitochondrial membrane also rely on the transmembrane potential. Accumulation of mitochondrial calcium ($[Ca^{2+}]_m$) during normal physiological cell signaling represents an important physiological stimulus that enhances ATP synthesis (McCormack and Denton 1993).

Cellular processes associated with increased energy demand (e.g. muscular contraction or neuronal activity) are driven by increased cytosolic $[Ca^{2+}]$. This signal is also propagated to mitochondria, leading to increased ATP generation. However, if combined with oxidative stress, a high $[Ca^{2+}]_m$ can become a major pathological stimulus, opening the mitochondrial permeability transition pore (mPTP), releasing cytochrome c and promoting apoptotic or necrotic cell death (Duchen 2000; Brookes, Yoon et al. 2004; Duchen 2004). In conjunction with NO, $Ca^{2+}$ enhances cytochrome c dissociation from the mitochondrial inner membrane, blocking the respiratory chain at complex III and stimulating ROS

production (Jacobson and Duchen 2004). Mitochondrial $Ca^{2+}$ uptake depends on both cytosolic [$Ca^{2+}$] and $\Delta\psi_m$. A decrease in potential may thus decrease mitochondrial $Ca^{2+}$ uptake. Surprisingly, in view of its importance in signaling, energy regulation and cell death, this has not been previously assessed in sepsis. While intracellular $Ca^{2+}$ dysregulation has been described in septic models (reviewed by (Rudiger and Singer 2007) and (Sayeed 2000)), alterations in $[Ca^{2+}]_m$ remain to be investigated.

### 1.3.4 Mitochondrial dysfunction in sepsis

Mitochondrial dysfunction can affect cellular function through the following processes (Callahan and Supinski 2009):

1. Reduced availability of high-energy phosphates, leading to a cellular metabolic crisis
2. Increased production of reactive oxygen species, resulting in damage to proteins and organelles (covered in 1.3.1.3);
3. Caspase activation and induction of apoptotic pathways by release of cytochrome C. In sepsis this is likely to be more important in immune cells and the gut epithelium (Ayala, Wesche-Soldato et al. 2007), than in other organs where little to no apoptosis is seen (Hotchkiss, Swanson et al. 1999; Langenberg, Bagshaw et al. 2008).

The current knowledge base of sepsis-induced mitochondrial dysfunction based around the various components of oxidative phosphorylation is described below.

#### 1.3.4.1 Electron transport chain dysfunction

Varying degrees of respiratory chain dysfunction have been reported in human and animal studies of sepsis. This is dependent upon sepsis severity, duration of illness and the organ studied (Brealey and Singer 2003). Few human studies have been reported. The largest series to date, studying patients with septic shock (compared to age-matched control patients undergoing elective hip surgery), showed reduced maximal activity of complex I in homogenates of skeletal muscle biopsied within 24 hours of ICU admission (Brealey, Brand et al. 2002). This inhibiton was greater in patients who eventually died, and was associated with higher nitrite/nitrate levels and lower tissue ATP levels. Of note, complex IV activity was increased. In another study, healthy volunteers given bacterial LPS underwent muscle biopsy at 2 and 4 hours (Fredriksson, Fläring et al. 2009). The investigators noted increased mitochondrial citrate synthase and complex I activities, implying that mitochondrial activity may be increased during the early stages of sepsis, although no changes in ATP or other high-energy phosphate levels were seen.

Most animal models of sepsis are based on rodents treated with LPS or by caecal ligation and puncture, with varying degrees of fluid resuscitation and organ dysfunction (Fredriksson and Rooyackers 2007). The results generally show similar findings of reduced respiratory chain activity that correlates with clinical severity (Crouser, Julian et al. 2002; Brealey, Karyampudi et al. 2004; Callahan and Supinski 2005). Addition of succinate to increase flux through complex II of the respiratory chain,

bypassing complex I inhibition, restored respiratory function in skeletal muscle taken from a rat model of sepsis (Protti, Carré et al. 2007).

Crouser *et al* (Crouser, Julian et al. 2002) showed reduced state 3 respiration (ADP dependent respiratory rate) in liver mitochondria isolated from LPS-treated, fluid resuscitated cats. Similar findings were found in rats injected with intraperitoneal LPS, where reduction in diaphragm muscle mitochondrial oxygen consumption was noted along with a selective depletion of mitochondrial complexes I, III, IV and V subunits (Callahan and Supinski 2005). My host lab reported a fall in mitochondrial respiratory proteins and transcript levels in patients with severe sepsis, that correlated with reduced functional capacity of the mitochondria (Carré, Orban et al. 2010).

#### 1.3.4.2 Mitochondrial transmembrane potential ($\Delta\psi_m$)

Compared to healthy controls, a higher percentage of monocytes isolated from severely septic patients had depolarised mitochondria Adrie *et al* (Adrie, Bachelet et al. 2001). This percentage was greater in eventual non-survivors. Hepatocytes isolated from LPS-treated rats also had a lower $\Delta\psi_m$ than controls (Růzicka, Skobisová et al. 2005).The percentage of viable hepatocytes isolated from the septic rats was also 20% lower than controls, implying a higher degree of fragility of cells.

#### 1.3.4.3 ATP Synthase defect

ATP synthase protein abundance decreased after six hours in

hearts isolated from rats treated with endotoxin (Robichaud, Lalu et al. 2009). This was accompanied by decreased activity of enzymes of the glycolytic and β-oxidation pathways. Callahan *et al* (Callahan and Supinski 2005) also reported reductions in the beta subunit of ATP synthase in skeletal muscle of LPS-treated rats.

#### 1.3.4.4 Uncoupled respiration

Porta *et al* (Porta, Takala et al. 2006) found increased state 4 (ADP-independent) mitochondrial respiration in liver mitochondria isolated from endotoxic pigs. Kidney and skeletal muscle mitochondria were unaffected, signifying differing responses between organs. Brain homogenates from mice who underwent caecal ligation and puncture showed higher state 4 respiration compared to sham controls (d'Avila, Santiago et al. 2008), with reduced respiratory control ratios (ratio of state 3:state 4 respiratory rates where lower ratios signify higher uncoupled respiration), and reduced ADP:O ratios (amount of ATP synthetized per unit oxygen consumption). They suggested that reduced coupling efficiency of oxidative phosphorylation was a potential mechanism underlying septic encephalopathy.

While most of the above studies have focussed upon mitochondrial function in whole tissue homogenate or isolated mitochondria, few have been performed in living intact cells or tissues isolated from septic humans or animals. Mitochondria do not work in isolation (Fig. 1.5). ATP production is governed by demands of energy-requiring cellular

processes, and by availability of substrate and oxygen. Regulatory mechanisms (involving, e.g., NO and intracellular $Ca^{2+}$) alter and perhaps fine-tune their function. Most physiological studies of isolated mitochondria define their maximal functional capacity. This may not be necessary for “normal” cellular function, but may potentially be needed when extra strain is placed upon the cell, requiring an increase in metabolic flux. Therefore, a major aim of my project was to develop techniques to study cellular and mitochondrial physiology (e.g. $\Delta\psi_m$) in living cells and tissues isolated from sick septic animals, and to correlate these with function in isolated mitochondria.

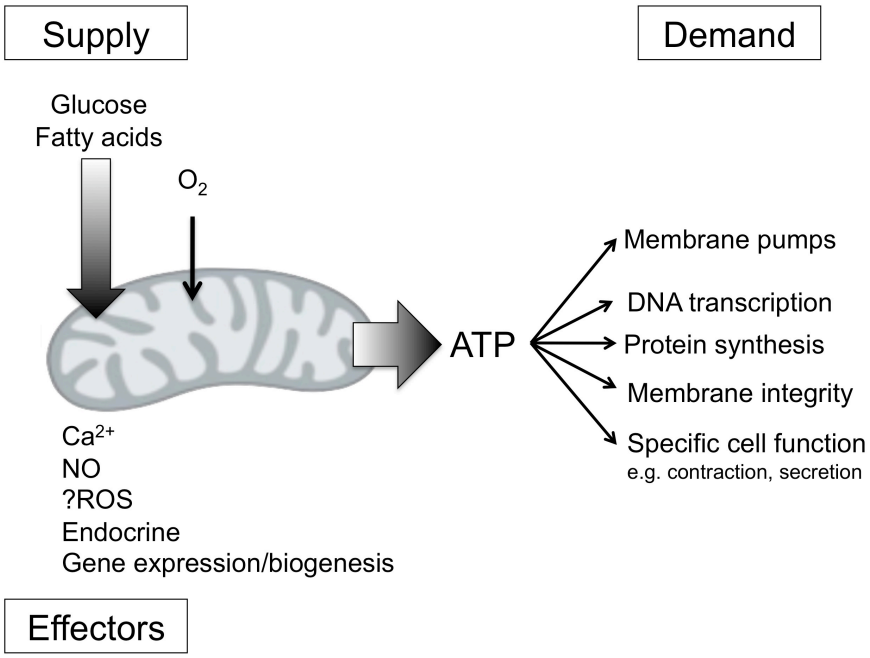


**Figure 1.5** Metabolic supply/demand regulation of mitochondrial function. Mitochondrial respiration is governed by the amount of available substrate and the demand for high energy phosphate. Regulatory mechanisms alter mitochondrial respiration while gene expression affects the abundance of mitochondrial protein. $Ca^{2+}$ increases flux through the respiratory chain by stimulating the dehydrogenases of the Krebs' cycle, whereas NO inhibits respiration at complexes I and IV.

### 1.4 The uncoupling proteins (UCPs)

These anion membrane transporter molecules are located within the mitochondrial inner membrane. While UCP-1 function is generally well understood, the (patho)physiological roles of UCP-2 and -3 remain uncertain. UCP-2 and -3 both share 57% homology with UCP-1, and are

found in cells and tissues that are crucial for energy expenditure, metabolism and immune function (Pecqueur, Alves-Guerra et al. 2001). UCP-2 is widely expressed in most mammalian tissues (Fleury, Neverova et al. 1997), while UCP-3 is predominantly expressed in fat, skeletal and cardiac muscle (Boss, Samec et al. 1997). Expression of UCPs increases with starvation and sepsis, and are associated with conditions such as insulin resistance in diabetes and atherosclerosis (Cadenas, Buckingham et al. 1999; Blanc, Alves-Guerra et al. 2003; Chan and Harper 2006). However, their impact on body metabolism remains poorly understood.

### 1.4.1 Genetic manipulation of UCP-2 and -3

Early work looking at over-expression of UCP-2 (Fleury, Neverova et al. 1997) and UCP-3 (Gong, He et al. 1997) in yeast and mammalian cell lines showed marked mitochondrial uncoupling with lowered $\Delta\psi_m$. However, over-expression of UCP mRNA (up to 66-fold), resulting in very high levels of protein, can significantly impact upon the integrity and structure of the inner mitochondrial membrane, resulting in an artefactual increase in proton conductance (Stuart, Harper et al. 2001; Cadenas, Echtay et al. 2002).

Studies using UCP-2 and -3 knockout mice are inconsistent (Nedergaard and Cannon 2003)). Reduced proton leak was found in thymocytes of *Ucp2*$^{(-/-)}$ mice (Krauss, Zhang et al. 2002), and skeletal muscle from *Ucp3*$^{(-/-)}$ mice (Vidal-Puig, Grujic et al. 2000). There was a concomitant increase in skeletal muscle ATP synthesis *in-vivo* in *Ucp3*$^{(-/-)}$

mice (Cline, Vidal-Puig et al. 2001). However, Cadenas *et al* (Cadenas, Echtay et al. 2002) showed no changes in $O_2$ consumption rates, respiratory control ratios or proton conductance in muscle mitochondria. Of note, this study was carried out using backcrossed mice (Nedergaard and Cannon 2003).Neither *Ucp2*$^{(-/-)}$ nor *Ucp3*$^{(-/-)}$ mice showed distinct phenotypes compared to wild-type counterparts in terms of total body energy metabolism, weight regulation, exercise tolerance, fatty acid oxidation and cold-induced thermogenesis (Arsenijevic, Onuma et al. 2000; Gong, Monemdjou et al. 2000; Vidal-Puig, Grujic et al. 2000).

### 1.4.2 UCPs and ROS production

Macrophages isolated from *Ucp2*$^{(-/-)}$ mice exposed to *Toxoplasma gondii* produced more ROS while the mice had lower levels of inflammation and infection than their wild-type counterparts (Arsenijevic, Onuma et al. 2000). Vidal-Puig *et al* (Vidal-Puig, Grujic et al. 2000) reported higher ROS production in skeletal muscle mitochondria of *Ucp3*$^{(-/-)}$ mice. Mitochondrial uncoupling leads to a higher flux of electrons through the respiratory chain, resulting in diminished ROS production (Korshunov, Korkina et al. 1998). In *Ucp3*$^{(-/-)}$ mice, the lack of UCP-3 protein should therefore result in lower uncoupled respiration, but with increased ROS production (Vidal-Puig, Grujic et al. 2000).

UCP-2 and -3 attenuate mitochondrial ROS production by “mild-uncoupling” of oxidative phosphorylation in a negative feed-back loop [Fig 1.6] (reviewed in (Brand and Esteves 2005; Echtay 2007)). Proton leak in

rodent skeletal muscle mitochondria stimulated by superoxide or 4-hydroxynonenol (product of lipid peroxidation) (Echtay, Roussel et al. 2002; Aguirre and Cadenas 2010) was higher in mitochondria taken from starved rats and LPS-treated mice, where UCP-3 protein abundance was increased. No proton leak was inducible in mitochondria from *Ucp3*$^{(-/-)}$ mice while the addition of ROS scavengers such as superoxide dismutase and the UCP inhibitor, GDP (guanosine diphosphate) reversed the leak. Under physiological stress, inhibition of the electron transport chain leads to excess ROS production. ROS and its byproducts stimulate UCP activation leading to mild uncoupling of oxidative phosphorylation, with increased flux through the respiratory chain and reduction in transmembrane potential. These changes ultimately result in attenuation of ROS production.

This mechanism is not universally accepted. Johnson-Cadwell *et al* (Johnson-Cadwell, Jekabsons et al. 2007) used the protonophore, carbonyl-cyanide-p-trifluoromethoxyphenyl hydrazone (FCCP), to mildly uncouple neuronal mitochondria. The cells had been stressed by glutamate and exhibited increased mitochondrial ROS production. Addition of FCCP to mildly uncouple the mitochondria (<10mV reduction in $\Delta\psi_m$) resulted in little change in mitochondrial matrix ROS production but did diminish spare respiratory capacity with a detrimental effect on cell survival. In another study, starvation induced a five-fold rise in rat skeletal muscle UCP-2 and -3 mRNA and UCP-3 protein levels, yet no changes were noted in muscle mitochondrial proton leak (Cadenas, Buckingham et al. 1999). These results imply that UCP -2 and -3 do not

catalyse proton leak, or that they must be activated before they do so.

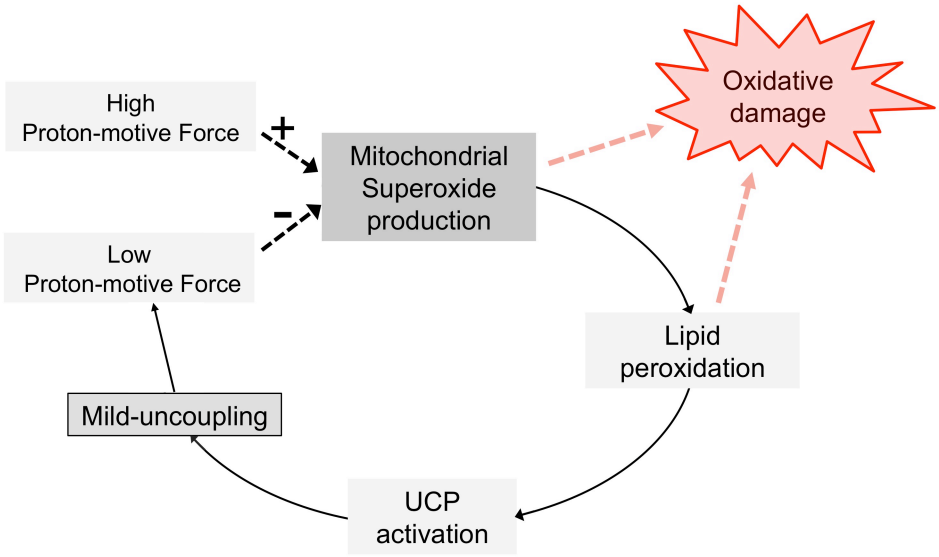


**Figure 1.6** Proposed "mild uncoupling" function of UCP-2 and -3 activated by superoxide or a lipid peroxidation by-product. Mild uncoupling leads to a reduction in transmembrane potential, thereby reducing availability of unpaired electrons of the respiratory chain to interact with $O_2$ to produce superoxide. This negative feed-back loop limits mitochondrial superoxide production.

Through their presumed function as mitochondrial uncoupling proteins, UCP-2 and 3 may play significant roles in non-shivering thermogenesis (reviewed by (Bézaire, Seifert et al. 2007)). However, compared to wild-type mice, no differences in core body temperature or metabolic response were found in *Ucp3*$^{(-/-)}$ mice in response to cold exposure (Vidal-Puig, Grujic et al. 2000), nor by injection of tri-

iodothyronine or a selective $\beta_3$-agonist into wild-type mice (both potent stimulators of uncoupling proteins) (Gong, Monemdjou et al. 2000). Cold exposure of arctic ground squirrels increased UCP-1 expression and protein abundance, but did not impact on UCP-3 expression (Barger, Barnes et al. 2006). *Ucp1*$^{(-/-)}$ mice are cold-sensitive yet their adipose tissue had no thermogenic properties, even though UCP-2 and -3 were still expressed (Enerbäck, Jacobsson et al. 1997). Under extreme adrenergic stimulation, such as hyperthermia induced by excess amounts of MDMA (3,4-methylenedioxymethylamphetamine), UCP-3 had a thermogenic role that was absent in *Ucp3*$^{(-/-)}$ mice (Mills, Banks et al. 2003; Mills, Rusyniak et al. 2004).

UCP-2 regulates insulin production through alterations in coupling efficiency of oxidative phosphorylation and ROS production (Affourtit, Jastroch et al. 2011). Increasing glucose levels results in a higher ATP/ADP ratio through oxidative phosphorylation in the pancreatic beta cells. This leads to closure of plasma membrane $K_{ATP}$ channels with depolarisation resulting in release of insulin (Rutter 2001). Acute knock-down of UCP-2 in INS-1 cells produced more insulin through more efficient oxidative phosphorylation. While this effect is apparent in cell models of glucose-stimulated insulin release, it is more discrepant in *Ucp2*$^{(-/-)}$ mice, likely due to metabolic adaptations and ROS damage (Affourtit and Brand 2008; Affourtit, Jastroch et al. 2011).

UCP-3 is involved in fatty acid metabolism (reviewed by (Brand and Esteves 2005; Bézaire, Seifert et al. 2007). UCP-3 expression is up-regulated in the presence of increased levels of fatty acids, e.g.

starvation. UCP-3 may transport excess fatty acids out of the mitochondrial matrix, thereby reducing potential toxicity from this accumulation. No such changes have been seen in *Ucp3*$^{(-/-)}$ mice. More controversially, UCPs have been implicated as a mitochondrial $Ca^{2+}$ uniporter (Trenker, Malli et al. 2007), although this is heavily disputed (Brookes, Parker et al. 2008).

In summary, the functional roles of UCP-2 and -3 are still not clearly understood. The most convincing evidence to date supports their role in attenuating mitochondrial ROS production, though their role in total body metabolism is likely to be minimal, at least in physiological states.

### 1.4.3 UCP-2 and -3 in sepsis

Sepsis is associated with significant increases in ROS production. According to the mild uncoupling theory, activation of UCPs by ROS results in mild uncoupling of electron transport from ATP production. This produces a modest degree of mitochondrial depolarisation, reducing ROS production while theoretically sustaining ATP production (Brand and Esteves 2005).

Of note, rats given endotoxin showed a three-fold increase in hepatocyte UCP-2 expression (mRNA and protein), and a reduction in $\Delta\psi_m$ (Růzicka, Skobisová et al. 2005). Increased UCP-2 expression was also reported in liver, white adipose tissue, skeletal and cardiac muscle (Faggioni, Shigenaga et al. 1998; Yu, Barger et al. 2000; Roshon, Kline et al. 2003). UCP-3 expression rose in skeletal muscle after 16-24 hrs of

sepsis (Faggioni, Shigenaga et al. 1998; Yu, Barger et al. 2000; Roshon, Kline et al. 2003; Sun, Wray et al. 2003). Faecal peritonitis in rats produced a 52% rise in myocardial UCP-2 mRNA abundance in cardiac muscle homogenates yet the actual protein was undetectable in mitochondria isolated from these hearts. This led to the conclusion that UCP-2 has no role in septic myocardial dysfunction (Roshon, Kline et al. 2003). A separate study involving LPS injection into young mice showed a five-fold rise in skeletal muscle UCP-3 expression while liver UCP-2 mRNA abundance dropped five-fold. Despite rises in UCP-3 expression, core temperature dropped to a nadir of 30°C (Yu, Barger et al. 2000). Compared to control mice no difference in proton leak kinetics of the mitochondrial isolated from liver and muscle were noted

The physiological response to sepsis has yet to be reported in *Ucp*$^{(-/-)}$ mice. It is unclear whether increased UCP expression in sepsis could be adaptive or maladaptive. Activation of UCPs could play a protective role by decreasing $\Delta\psi_m$, resulting in decreased ROS production. It may also have a profound effect on mitochondrial $Ca^{2+}$ accumulation that depends on $\Delta\psi_m$. It is equally plausible that increased UCP expression may decrease mitochondrial efficiency and ATP production, contributing further to the bioenergetic failure.

### 1.5 Skeletal muscle function in sepsis

Muscle weakness in the critically ill is a heterogeneous group of neuro-muscular disorders that is associated particularly with SIRS, sepsis

and multi-organ dysfunction (reviewed by (Deem, Lee et al. 2003; Hermans, De Jonghe et al. 2008)). A recent meta-analysis reported a 46% prevalence of critical illness polyneuropathy and myopathy (CIPNM) in patients who required prolonged mechanical ventilation (Stevens, Dowdy et al. 2007). CIPNM may be a neuromuscular manifestation of MOF with the same underlying pathophysiology, though other factors such as length of mechanical ventilation (Levine, Nguyen et al. 2008; Hermans, Agten et al. 2010), glycaemic control (van den Berghe, Wouters et al. 2001), and use of steroids and neuromuscular blocking agents may also contribute to its development and severity (Garnacho-Montero, Madrazo-Osuna et al. 2001; De Jonghe, Sharshar et al. 2002). CIPNM is associated with significant prolongation of weaning from mechanical ventilation (De Jonghe, Bastuji-Garin et al. 2007; Hermans, Wilmer et al. 2007).

Severe sepsis with worsening multi-organ failure (SOFA scores ≥10) is associated with reduced muscle force generation (Eikermann, Koch et al. 2006). The maximum force of contraction was half to one third of the evoked muscle force in healthy volunteers who had undergone a two-week period of limb immobilization. Interestingly, unloading the diaphragm and peripheral muscles during mechanical ventilation, as well as starvation alone, result in respiratory (Lewis and Sieck 1990; Levine, Nguyen et al. 2008) and peripheral muscle atrophy (Le Bourdelles, Viires et al. 1994). However, this did not result in reduced force generation. Muscle atrophy is commonly seen in sepsis, but does not account for all the changes seen in muscle function.

### 1.5.1 Mechanism of septic skeletal muscle dysfunction

Fatigue and decreased muscle strength of the diaphragm and respiratory muscles were first described in spontaneously breathing dogs and ventilated rats made endotoxaemic (Hussain, Simkus et al. 1985; Leon, Boczkowski et al. 1992). This was subsequently confirmed in other septic models (e.g. (Boczkowski, Vicaut et al. 1992; Supinski, Nethery et al. 1996; Fujimura, Sumita et al. 2000) and ICU patients (Cohen, Zagelbaum et al. 1982). Mechanisms underlying septic muscle dysfunction are multi-factorial and summarized in Figure 1.7 (reviewed by (Lanone, Taillé et al. 2005; Callahan and Supinski 2009). Increases in circulating pro-inflammatory cytokines are amplified in skeletal muscle tissue leading to increased production of ROS and RNS, and alterations in protein turnover and proteolysis (Wilcox, Osborne et al. 1992; Wilcox, Milliken et al. 1996). These changes are coupled with microcirculatory abnormalities (Boczkowski, Vicaut et al. 1992), and early reductions in tissue $pO_2$ that recover later in the course of sepsis (Dyson, Bezemer et al. 2011). Production of reactive species are associated with alterations in protein function (Nethery, DiMarco et al. 1999; Callahan, Stofan et al. 2001), reduced sensitivity of the contractile apparatus to $Ca^{2+}$ as well as sarcolemmal damage, altered membrane excitability and sodium channel abnormalities ((Lin, Ebihara et al. 1998; Rossignol, Gueret et al. 2007), review by (Lanone, Taillé et al. 2005)).

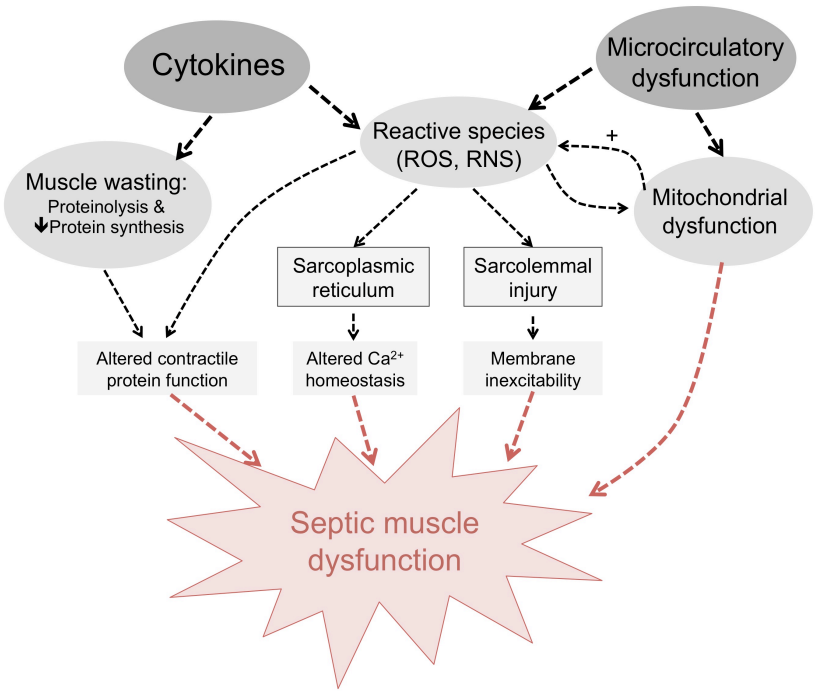


**Figure 1.7** The pathophysiology of septic muscle dysfunction is multi-factorial. Increased cytokine levels, early tissue hypoxia and increased ROS/RNS production are likely orchestrators. Contractile dysfunction results from altered protein metabolism and gene expression, bioenergetic dysfunction, sarcolemmal injury, altered ion channel activity and $Ca^{2+}$ dysregulation.

### 1.5.2 Inracellular $Ca^{2+}$ in septic muscle dysfunction

Few studies have investigated skeletal muscle $Ca^{2+}$ signaling in sepsis. Calcium is a vital part of excitation-contraction coupling. Plasma membrane depolarisation at the start of muscle contraction results in an influx of $Ca^{2+}$. This leads to further large release of $Ca^{2+}$ from the sarcoplasmic reticulum (SR) [cellular $Ca^{2+}$ stores] in a process termed $Ca^{2+}$-induced $Ca^{2+}$ release. This is stimulated through ryanodine receptors present on the SR. Released $Ca^{2+}$ causes conformational

changes in the actin and myosin filaments resulting in muscle contraction. Contraction is terminated by the re-uptake of intracellular $Ca^{2+}$ by the SR through an energy-dependent ionic pump, the sarco-endoplasmic reticulum $Ca^{2+}$ ATPase (SERCA) [see review by (Berchtold, Brinkmeier et al. 2000)].

Regulation of $Ca^{2+}$ homeostasis in muscle contraction is vital, however relevant studies in sepsis are scanty and inconclusive. Benson *et al* (Benson, Hasselgren et al. 1989) described higher skeletal muscle cell $Ca^{2+}$ levels in sepsis. Reduced re-uptake of $Ca^{2+}$ and higher SR $Ca^{2+}$ leak were reported in hearts of endotoxin-treated rats, leading to mitochondrial $Ca^{2+}$ overload and resultant metabolic failure (Hassoun, Marechal et al. 2008). Diaphragms isolated from endotoxic mice showed reduced peak tension development to both $Ca^{2+}$ and ryanodine stimulation, implying an abnormal $Ca^{2+}$ response at the SR (Liu, Lai et al. 2002). SR $Ca^{2+}$ release is sensitive to NO (Mészáros, Minarovic et al. 1996), so this may be a further potential mechanism affecting SR function in sepsis. Furthermore, reduced sensitivity of the contractile apparatus, again as a consequence of reactive species damage, may also contribute to changes in $Ca^{2+}$ signaling (Supinski, Nethery et al. 2000). Interestingly, Zink et al (Zink, Kaess et al. 2008) described reduction in $Ca^{2+}$ release by the SR of skeletal muscle isolated from septic mice. However, contrary to other studies, they reported an increase in contractile apparatus sensitivity to $Ca^{2+}$.

### 1.5.3 Muscle fatigue in sepsis

Respiratory muscle fatigue (decreased force/power generation during or after prolonged or repeated stimulation of muscle contraction (Place, Yamada et al. 2010)) likely contributes to respiratory failure in sepsis (Hussain 1998). In rodent models of sepsis, repeated phrenic nerve stimulation resulted in decreasing force of diaphragm muscle contraction with prolonged relaxation time, but preserved electrical activity (Lanone, Taillé et al. 2005).

In vitro muscle fatigue occurs in a characteristic triphasic pattern (Figure 1.8). Four potential mechanisms have been proposed (reviewed by (Place, Yamada et al. 2010)):

- extracellular $K^+$ accumulation
- muscle acidosis and increasing lactate accumulation
- increasing Pi concentration
- increased ROS/RNO production

Skinned muscle fibre experiments showed that both extracellular $K^+$ accumulation and increased lactate levels have minimal contributions to muscle fatigue (except at lower temperatures) (Zhang, Bruton et al. 2006; Allen, Lamb et al. 2008). Intracellular acidosis is thought to affect the rate of force relaxation (Westerblad, Bruton et al. 1997). Energy for muscle contraction is derived from breakdown of ATP to ADP and inorganic phosphate (ATP ➔ ADP + Pi). With repeated contraction, [ATP] is maintained by breakdown of phosphocreatine to creatine (PCr + ADP ➔ ATP + Cr), and the reaction of two ADP molecules to form ATP and AMP (2ADP ➔ ATP + AMP) (Allen, Lamb et al. 2008). This results in a

net reduction in [PCr], but a rise in [Cr] and [Pi]. The rising [Pi] is thought to enter the SR and precipitate with $Ca^{2+}$, thereby reducing $[Ca^{2+}]_i$ and resulting in a reduced force of contraction (Fryer, Owen et al. 1995; Westerblad and Allen 1996). Mitochondrial recruitment serves to maintain ATP levels, but even this is exhausted with continuing stimulation. In exercise, increased ROS levels have both a time-dependent and concentration effect on myofibrillar $Ca^{2+}$ sensitivity leading to development of fatigue (Andrade, Reid et al. 2001).

Fredriksson *et al* (Fredriksson, Hammarqvist et al. 2006) showed reduced levels of PCr and ATP and an increased lactate concentration in leg muscles of patients with sepsis. Lower ATP levels in skeletal muscle of severe septic patients were associated with reduced mitochondrial complex I activity and worse outcomes (Brealey, Brand et al. 2002). Depletion of reduced glutathione (antioxidant mechanism) and higher nitrite/nitrate levels signify increased reactive species production (Brealey, Brand et al. 2002; Brealey, Karyampudi et al. 2004). This is supported by studies showing higher cellular markers of ROS damage (Callahan, Stofan et al. 2001), (Andrades, Ritter et al. 2011), and that administration of intracellular anti-oxidants can prevent contractile and mitochondrial dysfunction (Dare, Phillips et al. 2009).

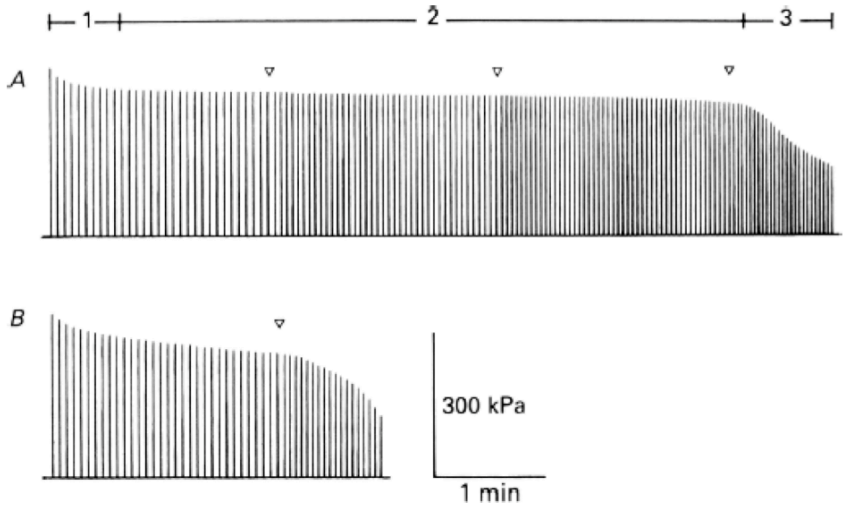


**Figure 1.8** The characteristic triphasic pattern of muscle fatigue seen in this force trace of repeated tetanic stimulation (350 ms) of mouse flexor digitorum brevis (A). A rapid decline in force generation is accompanied by increased $[Ca^{2+}]_i$ in phase 1. This likely represents rapid use of stored ATP and PCr. Force generation then reaches the plateau phase 2 where oxidative phosphorylation is recruited. This phase is shortened by mitochondrial inhibition following addition of cyanide (B), or in hypoxic conditions. Reduction in $[Ca^{2+}]_i$ as a result of increasing inorganic phosphate ($P_i$) concentration and $Ca^{2+}$-$P_i$ precipitation in the SR, as well as reduced myofibrillar $Ca^{2+}$ sensitivity rapidly deceases force generation in phase 3. (Figure from (Lännergren and Westerblad 1991)).

## 1.6 Animal models of septic organ failure

To investigate the pathophysiology of sepsis and novel therapeutic strategies, numerous animal models have been developed. However, there are substantial differences in physiological responses, not only between animal and human, but also between different investigators

using similar models. This might explain why many therapeutic agents that showed promise in animal models subsequently proved ineffective or even harmful in humans (reviewed by (Buras, Holzmann et al. 2005)). Rodent models are by far the most studied, but no standardized model of disease has been established that accurately reproduces the relevant physiological changes seen in patients with sepsis (Piper, Cook et al. 1996).

Hollenberg *et al* (Hollenberg, Dumasius et al. 2001; Hollenberg 2005) described a caecal ligation and puncture (CLP) model of mouse faecal peritonitis where aggressive fluid resuscitation (50ml/kg of 0.9% saline s/c 6 hourly) and antibiotic therapy reproduced the classic hyperdynamic state seen in human sepsis and improved 48-hour survival (46% vs. 0% in untreated animals). Miyaji *et al* (Miyaji, Hu et al. 2003) also used fluid and antibiotics to improve early survival in aged mice undergoing CLP. Their fluid regimen was less aggressive but they did also show biochemical and histological evidence of organ failure.

Few animal studies of sepsis have measured markers of organ dysfunction, attempted fluid resuscitation or stratified animals by the clinical severity of illness. My host lab developed an awake, long-term model of faecal peritonitis (Brealey, Karyampudi et al. 2004) in which rats were resuscitated with i/v fluids delivered continuously via an internal jugular vein catheter. Animals were stratified by severity of illness using easily measureable clinical parameters, with the severely ill animals displaying biochemical evidence of MOF. Importantly, no antibiotics were used in this model as antibiotics can alter mitochondrial protein synthesis

and transport processes (Zhang, Ging et al. 2005; McKee, Ferguson et al. 2006; Duewelhenke, Krut et al. 2007).

Physiological changes seen in animal models of sepsis are also influenced by the animal species, age, sex, co-morbidities, and type and severity of the insult (reviewed by (Dyson and Singer 2009)). Rodents are more resistant to LPS than larger animals and humans. LPS models have therefore been criticized as the higher doses used in rodents may produce toxic effects other than their immunostimulatory effects (Piper, Cook et al. 1996). CLP and live bacteria models produce severe forms of sepsis and more closely mimic “real life” polymicrobial sepsis.

The incidence of sepsis increases with age, peaking at 65 years in large American and European studies (Angus, Linde-Zwirble et al. 2001; Padkin, Goldfrad et al. 2003). This is equivalent to an age of 18 months in mice (Turnbull, Wlzorek et al. 2003). Similar to humans, older rodents are more susceptible to the effects of endotoxin (Tateda, Matsumoto et al. 1996) or polymicrobial sepsis (Turnbull, Wlzorek et al. 2003). However, due to cost constraints, most rodent studies of sepsis are performed in younger animals. Likewise, the incidence and outcomes from sepsis are also worse in males as a result of immunoregulation by oestrogen in the female sex (Diodato, Knöferl et al. 2001).

In summary, establishing a sepsis model identical to the human form of the disease is difficult and a degree of compromise is necessary. It is also important to consider the factors discussed above that can potentially influence the results.

## 1.7 Project aims

Sepsis is associated with significant changes in whole body metabolism, and with mitochondrial pathology. This has been proposed as an important pathophysiological mechanism underlying MOF. Most supporting data are from heterogenous models of disease, using mitochondrial preparations or whole tissue homogenates where the interdependence of mitochondrial function on cytoplasmic substrate supply and cellular ATP demand are disrupted. The aim of my thesis was to study mitochondrial function in an intact cellular environment within living tissues freshly isolated from septic animals. I placed particular emphasis on measuring mitochondrial transmembrane potential through novel fluorescent live-cell imaging techniques.

I felt it was important to first establish and optimize a reproducible mouse model of sepsis. This required characterization of the septic insult, fluid resuscitation regimen and measurement of organ dysfunction and physiological changes that occur from induction of sepsis through to death or resolution. By using more robust work-loop stimulation/relaxation cycles that mimic *in-vivo* muscle activity, diaphragm muscle force, power generation and fatigue was studied. A significant amount of time was also dedicated to developing methods to study $[Ca^{2+}]_i$ and $[Ca^{2+}]_m$ using live-cell fluorescent imaging.

Little is known about the dynamics of oxidative phosphorylation and proton leak in sepsis. UCP-3 is upregulated in sepsis, but the cellular and metabolic consequences are poorly understood. No studies have incorporated *Ucp-3*$^{(-/-)}$ mice. Increased UCP-3 expression may be

adaptive, limiting ROS production, or maladaptive resulting in partial dissipation of $\Delta\psi_m$ (through mild uncoupling and increased proton leak) when mitochondrial capacity is already critical. Therefore, the impact of UCP-3 deletion on survival from sepsis, as well as cardiovascular, metabolic and muscle dysfunction were also investigated. Proton leak kinetics and mitochondrial ROS production were also measured in isolated mitochondria and compared to naïve and sham mice.

# CHAPTER 2. MURINE MODEL OF SEPSIS

## 2.1 Introduction

Rodent models are routinely used to investigate both the patho-physiology of sepsis and novel therapeutic strategies. They attempt to mimic the human condition, yet significant differences are seen in physiological responses (Buras, Holzmann et al. 2005). Nevertheless, mouse models of sepsis have gained increasing favour due to transgenic technologies that allow manipulation of the genotype to test whole animal and cellular responses to the absence or over-expression of specific proteins (Haouzi 2011).

My host lab previously developed an awake, long-term (3-day) rat model of faecal peritonitis (Brealey, Brand et al. 2002) whereby animals were resuscitated aggressively with continuous intravenous fluid infused via a cannula inserted into the internal jugular vein. Severely affected animals showed biochemical evidence of organ failure. A similar model had been developed in C57 black mice, but had not been fully evaluated and optimized. In particular, the mouse model needed to be reproducible (to reduce number of animals used), develop septic multi-organ failure, and allow easy severity stratification using clinical signs.

I used this model to carry out a top-down examination of whole animal, tissue and cellular metabolism in sepsis, and to investigate the impact of an absence of UCP3 protein. Although the metabolic response to sepsis induced by bacterial peritonitis or endotoxin have been reported

in mice (Yu, Barger et al. 2000; Leon 2004; Valencia, Sarma et al. 2005), no descriptions have been made in conjunction with multi-organ failure, cardiac dysfunction or after standard therapies such as fluid resuscitation. Furthermore, development of hypothermia in septic mouse models is known to depend on ambient temperature (Rudaya, Steiner et al. 2005), yet it is unclear how ambient temperature or correction of body temperature affects the whole body metabolic rate.

In this chapter, whole animal metabolic changes in sepsis and starvation are described and correlated with changes in core temperature (before and after artificial re-warming to normal physiological levels), as well as changes in cardiovascular performance that affect tissue oxygen delivery. Cardiovascular reflexes were dynamically tested using fluid boluses to further define septic myocardial dysfunction to facilitate future studies using this model. These studies were carried out in wild-type C57 black mice and are compared to *Ucp3*$^{(-/-)}$ mice later in the thesis.

## 2.2 Methods

### 2.2.1 Animal model

Experiments were performed in accordance with the Animals (Scientific Procedures) Act 1986 and approval from the local Ethics Committee. Male, 18-30 week old C57 black mice (Charles River, Margate, UK), weighing 25-35g, were housed with 12-hour light and dark cycles and full access to food (standard chow) and water. Room

temperature was controlled at 21°C. All mice underwent a 7 day period of acclimatization in the laboratory prior to start of experiments.

#### 2.2.1.1 General anaesthesia (GA) for procedures

Mice were anaesthetized with isoflurane in an enclosed chamber, and transferred onto a heated mattress where anaesthesia was maintained with the mice breathing spontaneously through a facemask entrained with a mixture of air and isoflurane. This was achieved using a Tetratec Whisper® Air pump (Spectrum Brands, Cincinnati, Ohio, USA) set at 500ml/min connected to a Tec 3 Isoflurane vaporizer. The minimal depth of anaesthesia with mice breathing spontaneously but having lost withdrawal reflex to pain, was tailored to each mouse at each time-point.

#### 2.2.1.2 Original model of sepsis

This model was based on the awake rat model where insertion of tunneled intravascular lines (carotid artery and internal jugular vein) was followed 24 hours later by injection of faecal slurry (Brealey, Karyampudi et al. 2004).

Tunneled intravascular lines (PVC tubing 0.61mm outer diameter, 0.28mm inner diameter, Tyco, Victoria, Australia) were inserted into the right internal jugular vein and left carotid arteries under aseptic conditions and general anaesthesia. The lines emerged from the nape of the neck and passed through a cylindrical tether that was stitched to the skin of the

back. The end of the tether was attached to a pulley system so the mice could freely move around their cage and gain access to food and water.

Intravascular lines were kept patent by 0.1 ml/hr of heparinised saline (1 unit/ml). Blood pressure was continuously recorded using a pressure transducer. After 24 hours' recovery, 0.5 ml of diluted rat faecal slurry (1:7 dilution with 0.9% saline) prepared fresh was injected intraperitoneally into the septic group. No injection was made in the sham group to avoid accidental bowel injury. Fluid resuscitation commenced 2 hours after the i/p slurry injection with a 1:1 mix of 5% glucose and 6% hetastarch (Elohaes®, Fresenius-Kabi) at a rate of 0.3 ml/hr (10 ml/kg/hr). Glucose was added to the resuscitation fluid to avoid hypoglycaemia. At 24h the rate of infusion was halved. A clinical severity score validated in rats (Brealey, Karyampudi et al. 2004) was used to classify severity (Table 1).

A survival study carried out soon after development of this model revealed a very high mortality in the sham mice (33% mortality at 72 hrs [Fig 2.3]). This was felt due to the operative procedure to insert intravascular lines and perhaps stress related to being tethered, and prompted the development of a new model of sepsis.

(A)

| Clinical sign | Possible score |
|---|---|
| Hunched? | 0-1 |
| Bloated? | 0-1 |
| Mucky eyes? | 0-1 |
| Lack of alertness? | 0-2 |
| Lack of movement? | 0-2 |

(B)

| Severity of sepsis | Sum of clinical score |
|---|---|
| Mild | 0-2 |
| Moderate | 3-4 |
| Severe | 5-7 |

**Table 2.1 (A)** Clinical signs used to assess severity of illness, and **(B)** the severity of illness score based on the sum of the individual clinical signs.

#### 2.2.1.3 New model of mouse faecal peritonitis

The major change in the new model was the absence of tunneled intravascular lines, thereby removing the surgical insult, any post-operative pain and discomfort from the tether. Fluid resuscitation was instead carried out using subcutaneous (s/c) fluid. Other changes were:

- Injection of faecal slurry into the peritoneal cavity following direct visualisation of the abdominal musculature through a transverse skin incision under GA, ensured correct placement

of slurry. Sham animals had the same incision and injected with 0.9% saline. Wound was closed by a single stitch.

- 20ml/kg volume of i/p slurry (septic) or saline (sham).
- Fluid resuscitation at end of set-up procedure with 10ml/kg of 0.9% saline s/c.
- Further s/c fluid resuscitation using boluses of 50ml/kg of pre-warmed 5% glucose/0.81% saline at 6, 18, 30 and 42 h time-points under brief general anaesthesia.

The scoring system shown in Table 2.1 was used at 24h to define sepsis severity in each mouse. The score was evaluated against physiological and biochemical parameters described below.

Weight was recorded at 0 and 24 h. Core temperature and blood sugars were measured at 0, 6, 18 and 24 h time-points, immediately after induction of brief general anaesthesia and just prior to injection of the s/c fluid boluses. A thermistor (Thermilinear®, Yellow Spring Instruments, Ohio, USA) placed rectally (with tip of probe 1cm from anus) and coupled to an Ohm-meter was used to measure core temperature. Serum glucose was measured from blood obtained from a tail-snip. The same tail-snip was used for serial sampling by removing surface clot and massaging blood from the wound. Blood sugar was measured by an Ascensia Elite blood glucose monitor and test strips (Bayer, Mishawaka, USA). The instrument was regularly calibrated using manufacturer's instructions.

At 24 h, a group of mice (sham, mild, moderate and severe septic) were culled and 0.4-1 ml blood obtained by cardiac puncture. A small

volume of the blood was heparinised for blood gas analysis (ABL-70 analyzer, Radiometer, Copenhagen, Denmark). The remainder was allowed to clot for 10 mins. spun twice (1600g) to separate the serum and frozen at -20°C. Serum electrolytes, urea, creatinine, liver enzymes (alanine transaminase, aspartate transaminase, alkaline phsophatase), and albumin were measured by The Doctor's Laboratory, London.

### 2.2.2 Standardisation of the septic insult

Initial experiments with this model showed a wide weekly variation in septic response and survival. Faecal slurry comprises a range of pathogenic bacterial species that vary dependent on diet and bowel colonization. This may explain the weekly variation in response seen in the mice. Preparation of a fixed amount of live bacteria (evaluated by microbiological methods) represents a considerable logistic challenge. On the other hand, the caecal ligation and puncture model requires an additional operative procedure and introduces an ischaemic/infarcted tissue component to the septic insult.

To reduce the variability of the septic insult, I investigated the effect of freezing faecal slurry and defrosting at weekly intervals on the number and potency of the bacteria. I performed this study with help from Drs Sean Nair and Samantha Packer (Eastman Dental Institute, UCL). Two batches of slurry were prepared. One was diluted in 0.9% saline and the other in a mixture of saline and glycerol (20% final volume) as glycerol reduces damage to bacteria by the freeze-thaw process. These

batches were aliquoted into 1 ml cryotubes and stored at -80°C. Each week for five weeks, an aliquot from each batch was thawed. Half was plated on agar plates to quantify the viable anaerobic and aerobic bacterial populations. The other half was diluted further and injected intraperitoneally into two C57 black mice to test *in vivo* potency. Results (see 2.3.2) showed that bacterial numbers remained static yet the freeze-thaw process reduced bacterial potency.

During these experiments, I noted a more uniform response when the faecal slurry was made fresh and under more stringent conditions (dilution and storage in the fridge for <24 hours). I/p injection under direct vision (described above) also produced less variability.

### 2.2.3 Cardiac output measurement by echocardiography

Echocardiography was performed at 0, 3, 6 and 24h post-induction of sepsis. Sham-operated animals were used as non-septic controls. The mice were anaesthetized with isoflurane while breathing spontaneously. Severely ill animals and humans have lower anaesthetic requirements (Gill, Martin et al. 1995; Allaouchiche, Duflo et al. 2001). Therefore, the percentage of isoflurane was appropriately adjusted to maintain the same degree of anaesthetic depth, judged by loss of withdrawal reflex to pain as the reference point.

A 13MHz probe connected to a Vivid 7 echocardiography machine (GE Healthcare, Chalfont St.Giles, Bucks) was used to obtain a parasternal long axis view of the heart. Peak velocity (PV) and the

velocity time integral (VTI) were measured using pulsed wave Doppler in the ascending aorta proximal to branching of the major vessels (Fig. 2.1). The velocity time integral of the Doppler flow profile in the ascending aorta represents 'stroke distance' (SD), the distance a column of blood travels in the aorta during each systole (Fig. 2.13). Stroke volume is the product of stroke distance and aortic cross-sectional area. Aortic diameter was assumed to be 1.35mm, as measured in similar age and size mice using a 30MHz probe, (personal communication, Dr.Steve Hollenberg, Cooper Hospital, Camden, NJ, USA).

The peak velocity (PV) is a marker of myocardial contractility assuming normal valve and vessel structure. It is the peak of the Doppler flow profile (Fig. 2.13). Both PV and VTI have been validated in an open-chest mouse model (Hartley, Michael et al. 1995). Each measurement of PV and VTI was taken from the average of six Doppler envelopes.

Parasternal short axis views and M-mode echocardiograms of the left ventricle were obtained at the papillary muscle level to assess fractional shortening (Figs 2.12 & 2.13):

$$\text{Fractional shortening} = \frac{\text{End-diastolic diameter - end-systolic diameter}}{\text{End-diastolic diameter}}$$

Further experiments were performed to assess the response of the cardiovascular system to intravenous fluid boluses at 6h and 24h following induction of faecal peritonitis. Following general anaesthesia, the anterior skin of the neck was incised under aseptic conditions and the right internal jugular vein cannulated with PVC tubing (0.61mm outer

diameter x 0.28mm inner diameter, Tyco, Victoria, Australia). An Ultra-Miniature Mikro-Tip Pressure Transducer Catheter (1FG; Millar Instruments, Houston, Texas, USA) was introduced into the left carotid artery for real-time measurement of blood pressure. Mice were warmed during instrumentation to achieve a core temperature of 34-36°C.

Following a 10-minute period of stabilisation, a baseline echocardiogram was performed. Echocardiogram and blood pressure recordings were then made after serial fluid boluses of 0.5 ml of warmed hydroxyethyl starch solution (Voluven®, Fresenius Kabi, Germany) to a total of 3 ml. Each fluid bolus was administered over 3 minutes and echocardiogram performed immediately after each bolus. There was a 10-minute gap between each fluid bolus. These experiments were performed rapidly to minimize the effect of dilutional anaemia.

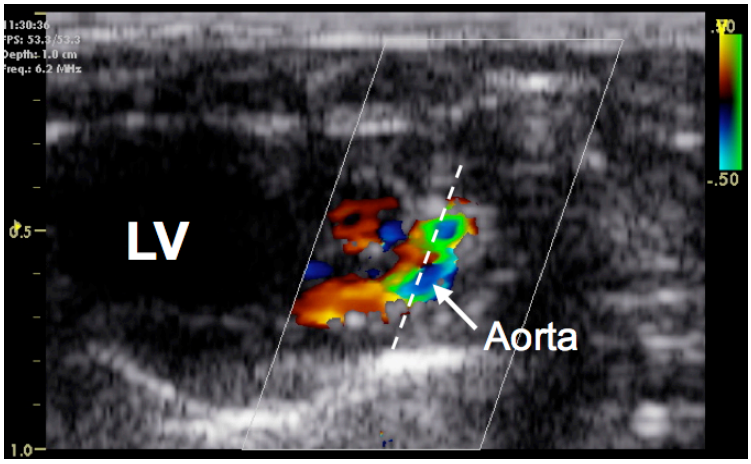


**Figure 2.1** Parasternal long axis echocardiogram of the mouse heart with colour Doppler showing the aortic arch and left ventricle (LV). The dotted line is the orientation of the cursor of pulsed wave Doppler; the cosine rule was used to correct for the angle of flow.

### 2.2.4 Measurement of whole body metabolic rate

Whole body metabolic rates were measured by placing mice into sealed metabolic chambers (Oxymax system, Columbus Instruments, Columbus, OH, USA) for the duration of the experiment (Fig 2.2).

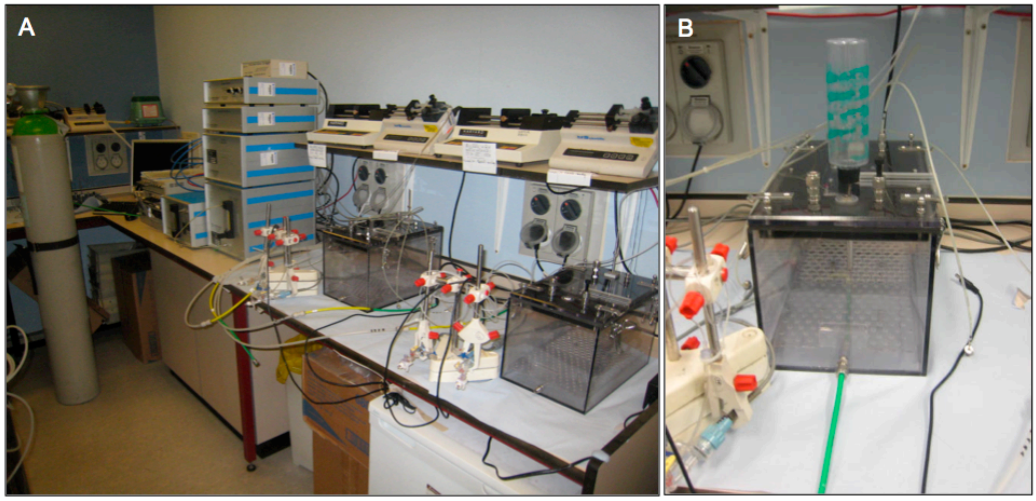


**Figure 2.2 (A)** The Oxymax system shown with two rat metabolic carts on the right and the central controller and gas analyzer boxes on the left. **(B)** A metabolic cart with gas inflow (green line) and outflow at the top with water bottle inverted into the cage. The boxes are fully sealed and gas flow in and out is controlled by a central controller.

The rig consisted of four chambers, allowing simultaneous recordings in four mice at any one time. Gas samples were analyzed from each box over a 90 second sampling period every 8 minutes. Oxygen consumption ($VO_2$) and $CO_2$ production ($VCO_2$) were calculated by applying the Fick principle using the concentration of gas pumped in and out of the box over the sampling period:

$\mathbf{VO_2 = V_i\ O_{2i} - V_o\ O_{2o}}$ ($V_i$ and $V_o$ are the input and output ventilation rates (LPM), $O_{2i}$ and $O_{2o}$ are oxygen fractions at the input and output)

$\mathbf{VCO_2 = V_o\ CO_{2o} - V_i\ CO_{2i}}$ ($V_i$ and $V_o$ are the input and output ventilation rates (LPM) $CO_{2i}$ and $CO_{2o}$ are carbon dioxide fractions at the input and output)

The respiratory exchange ratio (RER) was calculated as $VCO_2/VO_2$. This ratio indicates the predominant fuel being used to provide energy at a given time. Values near 1 indicate a predominance of carbohydrate metabolism while values near 0.7 indicate fatty acid oxidation (Jéquier, Acheson et al. 1987).

#### 2.2.4.1 The effect of re-warming on metabolic rate in sepsis

The effect of re-warming on total body metabolism was investigated by transferring the septic animals from their metabolic cages to a heated chamber (set to 38°C) for 1.5 hours. The animals were then quickly returned to their sealed boxes and recordings recommenced. Ideally, the re-warming should have occurred in the metabolic chamber, but this proved logistically and financially impossible.

Re-warming took place at 10h and 24h when metabolic down-regulation was fully established, and absorption of the subcutaneous fluids (injected at 6 and 18h) would have taken place. This reduced the risk of cardiovascular compromise upon re-warming. Echocardiograms

were performed to measure cardiac output before and after re-warming to assess changes in oxygen delivery (see later for detail).

## 2.3 Results

### 2.3.1 Survival in the original mouse model

Initial studies using the original model of sepsis were carried out using male 18-22 week old mice weighing 21-28 g. Experiments were performed in five batches spread over a two-week period with animals randomly allocated to sham and septic groups.

Mortality was 73% (8/11) in septic mice at 48 h (Fig. 2.3); most of the deaths occurring within 24 h. Crucially, there was a high mortality rate (33%) in the sham mice (3/9 dead), with signs of illness apparent in the 6 surviving sham mice (severity scores of 2-3). This suggested that the instrumentation procedure and/or the fluid regimen were hazardous.

The intra-arterial lines regularly became blocked due to their small calibre, with only two reliable continuous arterial pressure recordings achieved in the sham group and one in the septic group. No difference in mean arterial pressure (MAP) between the sham and septic recordings were found (both in the region of 100mmHg).

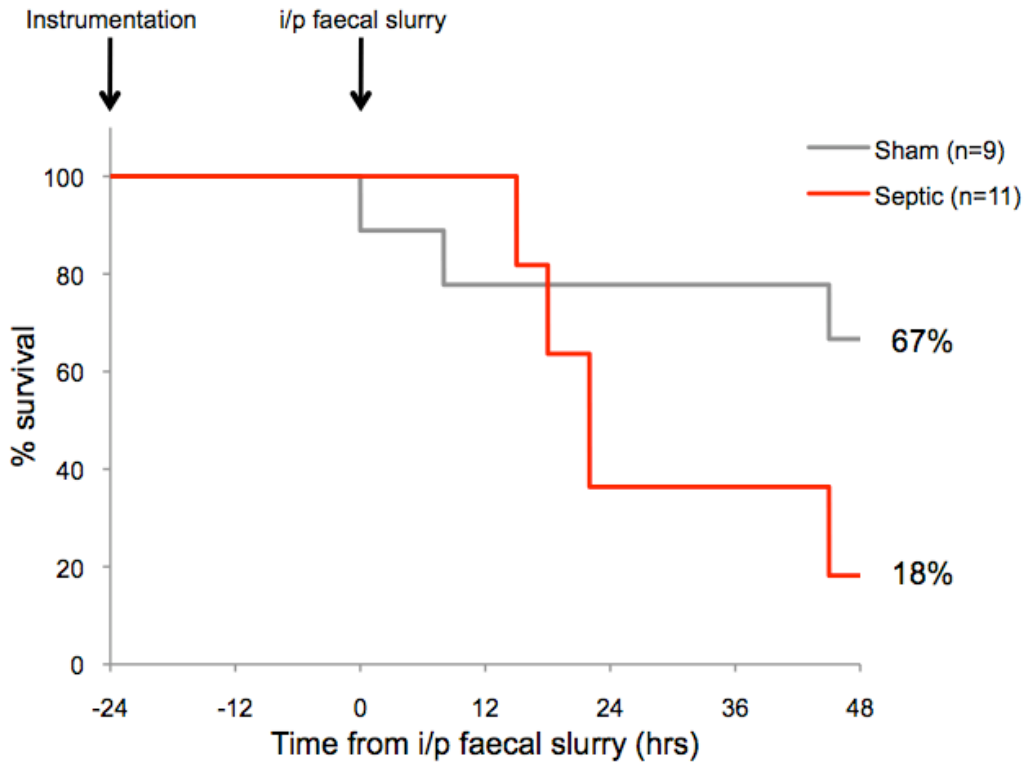


**Figure 2.3** Kaplan-Meier survival curve of sham and septic animals in the tethered, i/v fluid-resuscitated original model of sepsis. Mice had tunnelled intravascular lines inserted at the -24h time-point and were allowed to recover before receiving i/p faecal slurry (septic) or saline (sham) at 0h.

Coincidental with this initial work, another study in the host lab using this model failed to detect biochemical evidence of organ failure, even in severely ill animals. All these features were dissimilar from the rat model where healthy, surviving sham animals and sick septic animals with organ dysfunction were reliably obtained. Possible explanations include operator technique and differences in animal phenotype. This

latter phenomenon had previously been witnessed within the laboratory when colonies from new breeding pairs were established.

Further experiments were thus essential to redesign and refine the model in order to achieve:

i. healthy sham animals
ii. biochemical and functional evidence of organ dysfunction in the septic animals
iii. avoidance of intra-vascular lines as these yielded little useful data and the tether system in use at the time was unwieldy
iv. standardization of the septic insult
v. review of the fluid resuscitation regimen to prevent both hypovolaemia and potential volume overload

### 2.3.2 New mouse model of sepsis

The new model had no intravascular lines inserted. Instead, fluid resuscitation was performed by serial subcutaneous injection of fluid along with other optimisation steps (described in more detail below).

To standardise the septic insult, faecal slurry was diluted in saline or saline plus 20% glycerol, and stored at -80°C. The number of viable bacteria in the 0.9% saline group decreased by two log orders over a 3-week period, while the number of viable bacteria in 20% glycerol remained static, even after five weeks (Fig 2.4). However, despite this maintained viable bacterial count, *in vivo* testing indicated diminished potency over the five weeks (Table 2.2). This may be a direct result of

reduction in bacterial toxin titres with prolonged freezing (Freeman and Wilcox 2003).

Clearly, freezing faecal slurry was not a viable option. Instead, the following changes were made to the model:

i. Fresh faecal slurry made weekly with stringent conditions;
ii. Intraperitoneal injection of faecal slurry under direct vision;
iii. Weight-adjusted volume of slurry (20ml/kg);
iv. Subcutaneous fluid resuscitation regimen.

These changes resulted in a more predictable model of disease resulting in a reduced number of mice used but favouring a more severe disease.

Laparotomies performed on the septic mice at 24h showed varying degrees of stomach and bowel dilatation, pus and adhesions depending on the severity of sepsis. These findings were likely due to paralytic ileus and gastric stasis caused by peritoneal inflammation and irritation.

As close observation of feeding behaviour revealed that even the mildly septic animals stopped eating. Therefore, a new control group of starved sham mice was included where mice had access to water but not food following i/p injection of saline.

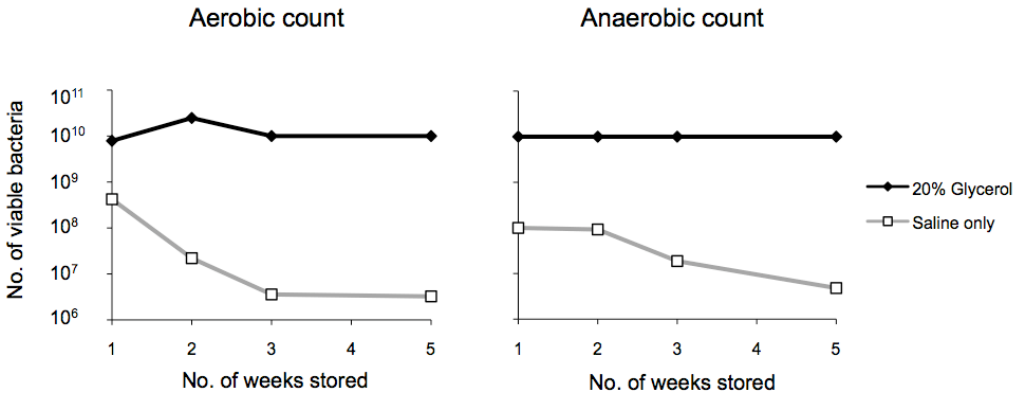


**Figure 2.4** Aliquots of slurry stored in either 20% glycerol or 0.9% saline at -80°C and thawed weekly to measure viable bacterial count.

| No of Weeks stored | Outcome | Clinical severity score at 48hrs |
|---|---|---|
| 1 | Mouse 1- dead (15 h)<br>Mouse 2- dead (23 h) | dead<br>dead |
| 3 | Mouse 1- survived<br>Mouse 2- dead (36 h) | 2<br>dead |
| 5 | Mouse 1- survived<br>Mouse 2- survived | 1<br>0 |

**Table 2.2** Outcome of mice receiving i/p injection of slurry preserved in 20% glycerol at -80°C. Severity score ≤2 mild, 3-4 moderate, ≥5 = severe

#### 2.3.2.1 Serum biochemistry at 24 hours

Following implementation of the above changes, blood samples were taken at 24h following induction of sepsis. These showed a graded rise in biochemical markers of renal and hepatic dysfunction with increasing severity of illness (Fig. 2.5):

i. serum urea and creatinine rose significantly (4- and 8-fold rise, respectively) in the severely septic mice ($p<0.05$);
ii. rise in liver transaminases (2-3 fold in severe mice, $p<0.05$);
iii. serum albumin levels were reduced by up to 28% in all septic groups when compared to fed sham animals receiving equivalent amounts of fluid ($p<0.05$).

#### 2.3.2.2 Arterial blood gases at the 24h time-point

Table 2.3 shows blood gas sample analyses taken by direct cardiac puncture soon after anaesthesia. Depth of anaesthesia had been adjusted to account for degree of hypothermia and severity of illness. A mixed metabolic and respiratory acidosis was seen in the severely septic animals. Interestingly, even naïve mice had a low serum bicarbonate ($[HCO_3^-]$ ~18 mmol/L) and high standard base deficits (-8 mmol/l). These findings persisted despite re-calibration of the analyser. Haemoglobin concentrations were higher in the severely septic mice, likely as a result of haemoconcentration due to capillary leak.

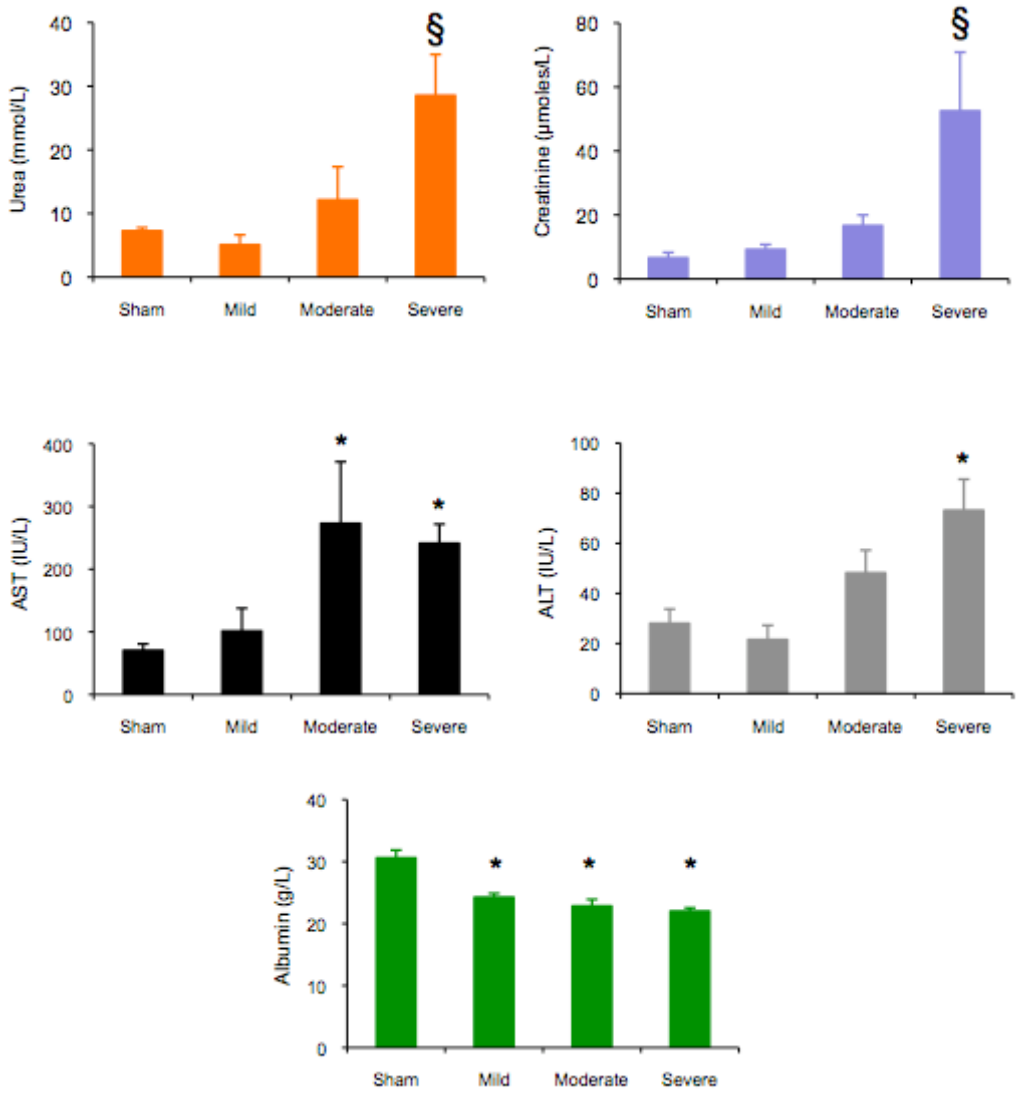


**Figure 2.5** Serum urea, creatinine, aspartate transaminase (AST), alanine transferase (ALT) and albumin taken from sham (n=5), mild septic (n=5), moderate septic (n=6) and severe septic (n=6) mice at 24 h.

§ $p<0.05$ when compared to sham and mild septic mice.

* $p<0.05$ when compared to sham mice.

| | Naive | Fed Sham | Starved Sham | Fed Severe | Starved Severe | P value |
|---|---|---|---|---|---|---|
| **N** | 6 | 2 | 4 | 3 | 7 | |
| **pH** | 7.31 ± 0.07 | 7.33 ± 0.01 | 7.34 ± 0.04 | 7.06 ± 0.06 * | 6.91 ± 0.11 * | <0.05 |
| **$pCO_2$ (kPa)** | 4.86 ± 0.93 | 4.66 ± 0.01 | 4.04 ± 0.58 | 6.65 ± 0.37 * | 9.23 ± 1.96 * ‡ | <0.05 |
| **$pO_2$ (kPa)** | 12.0 ± 3.2 | 14.0 ± 1.0 | 13.0 ± 5.9 | 14.4 ± 0.7 | 11.3 ± 5.0 | NS |
| **$HCO_3^-$ (mmol/l)** | 18.1 ± 2.0 | 18 ± 0 | 17.4 ± 0.5 | 14.1 ± 1.7 * | 8.9 ± 2.1 * ‡ | <0.05 |
| **BE (mmol/l)** | -7.7 ± 2.6 | -8 ± 0.0 | -8.8 ± 0.7 | -16 ± 2.6 * | -18.8 ± 3.2 * | <0.05 |
| **Lactate (mmol/l)** | 5.6 ± 0.4 | | 3.2 ± 0.4 § | | 4.5 ± 0.3 | <0.05 |
| **Hb (g/dl)** | 13.3 ± 0.4 | 13.1 ± 0.3 | 13.2 ± 0.3 | 13.3 ± 1.1 | 15.9 ± 1.2 * ‡ | <0.05 |
| **$Na^+$ (mmol/l)** | 147 ± 1 | | 147 ± 3 | | 147 ± 2 | NS |
| **$K^+$ (mmol/l)** | 4.9 ± 0.6 | | 4.3 ± 0.3 | | 4.4 ± 0.7 | NS |
| **$Cl^-$ (mmol/l)** | 116 ± 2 | | 123 ± 6 * | | 122 ± 2 * | <0.05 |

**Table 2.3** Results of blood gas analysis by direct cardiac puncture at 24h in sham, septic and naïve mice. Results shown as mean ± standard deviation. Statistical analysis was performed using one way ANOVA.

p<0.05 when compared to naïve, fed sham and starved sham.

‡ p<0.05 when compared to fed severe septic.

§ p<0.05 when compared to naïve and starved septic.

BE= Base Excess, Hb= Haemoglobin.

### 2.3.2.3 Blood glucose changes over 24 hours

Blood samples taken at 0, 6,18 and 24 hours following induction of sepsis showed no evidence of hypoglycaemia in this model. The lowest values were recorded in the starved severe septic animals where, at 6h and 18h, blood sugars were 5.2 ± 1.0 and 5.8 ± 1.4 mmol/l, respectively (Fig 2.6). Blood sugar at the 0h time-point was high (12.2±0.3 mmol/L) and may reflect stress caused to mice as a result of general anaesthesia and tail snipping.

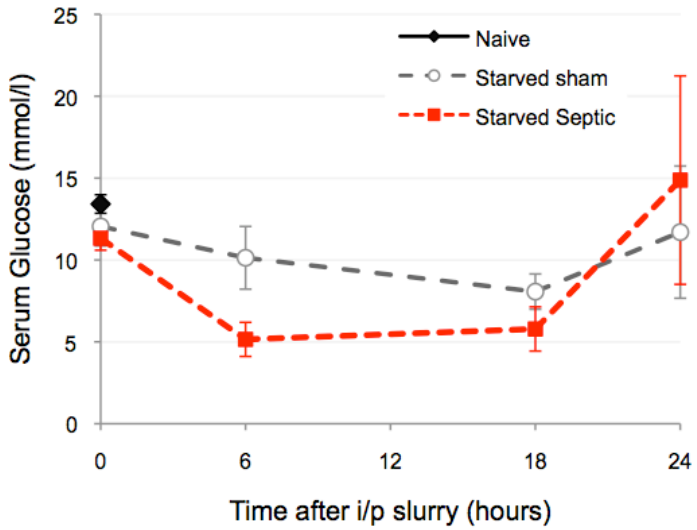


**Figure 2.6** Serum glucose in naïve, starved sham and starved severe septic animals over 24 hours. At 0h, i/p slurry was injected. A mixture of saline 0.81%/glucose 5% was injected s/c to all mice at 6h and 18h. Results are expressed as mean ± SD. There were 6, 4 and 8 mice in the naïve, starved sham and starved severe septic groups, respectively.

### 2.3.2.4 Effect of sepsis on body temperature in mice

Rectal temperatures measured immediately after induction of anaesthesia and at 0, 6, 18 and 24h following injection of faecal slurry (or saline injection for sham animals) are shown in Fig. 2.7. All septic mice exhibited a drop in temperature at 6 hours which was much more pronounced in the severely ill animals ($p<0.05$), and lower still in those that were concurrently starved ($p<0.05$).

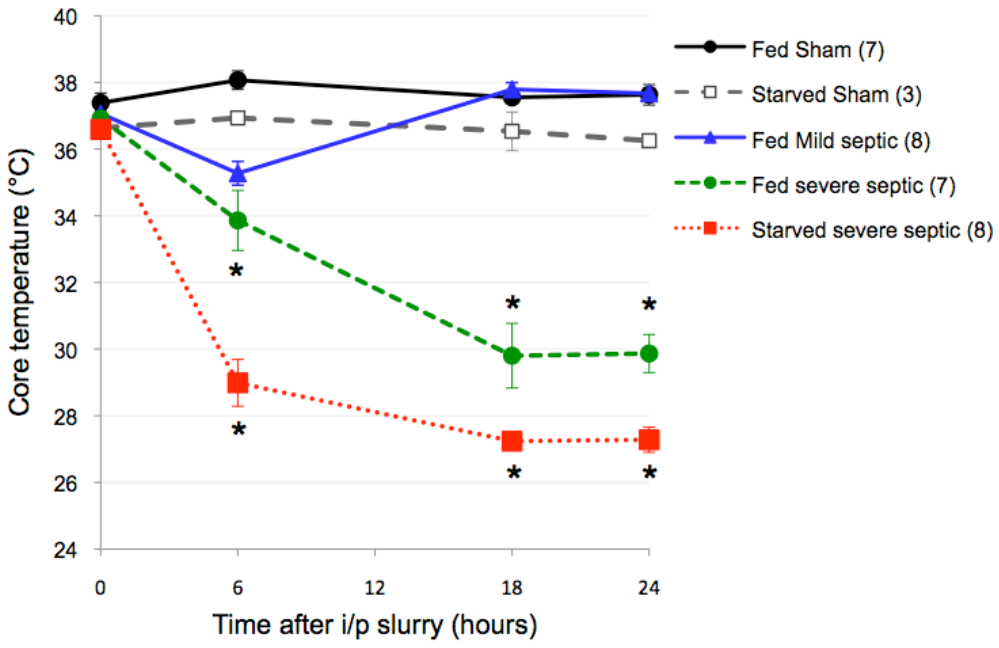


**Figure 2.7** Core temperatures of mice after injection of faecal slurry or saline at 0h. The number of mice per group is indicated in parentheses. Two-way ANOVA with Scheffe post-hoc analysis was used to describe the statistical relationship between the groups.

* indicates $p<0.05$ when compared to all groups.

### 2.3.2.5 Weight changes following induction of sepsis

As mentioned earlier, septic mice stopped eating. However, the severely septic mice actually *gained* weight over the 24 hours (weight gain of 4.2 ± 1.6% fed septic, 5.2 ± 0.8% starved septic) [Table 2.4]. Post-mortems carried out in these mice showed significant amount of sequestered fluid in subcutaneous spaces, as well as peritoneal/pleural effusions and distended bowel filled with fluid.

On the other hand, the mildly septic animals *lost* 6.2 ± 1.6% of their body weight and manifested little in the way of tissue oedema, ascites or pleural effusion fluid. Starvation in the sham animals led to a 7.5 ± 1% weight reduction despite the subcutaneous fluid (Fig 2.8). Fed sham mice showed no statistical weight change (-1.8 ± 1.3%; $p>0.05$).

| | Weight 0h (g) | Weight 24h (g) | Change in weight (g) | P value |
|---|---|---|---|---|
| **Fed Sham (7)** | 30.8 ± 1.2 | 30.2 ± 1.1 | -0.6 ± 0.4 | 0.161 |
| **Starved sham (10)** | 31.0 ± 1.1 | 28.7 ± 1.0 | -2.4 ± 0.3 | 0.000 |
| **Fed Mild Septic (9)** | 32.5 ± 0.9 | 30.4 ± 1.0 | -2.0 ± 0.5 | 0.006 |
| **Fed Severe Septic (9)** | 30.3 ± 0.9 | 31.6 ± 0.9 | 1.2 ± 0.4 | 0.018 |
| **Starved Severe Septic (17)** | 31.5 ± 0.9 | 33.0 ± 1.0 | 1.6 ± 0.2 | 0.000 |

**Table 2.4** Weight of mice at induction of sepsis (Weight 0h) and 24 hours (Weight 24h) after i/p faecal slurry or saline. Statistical analysis was performed using a paired sample t-test.

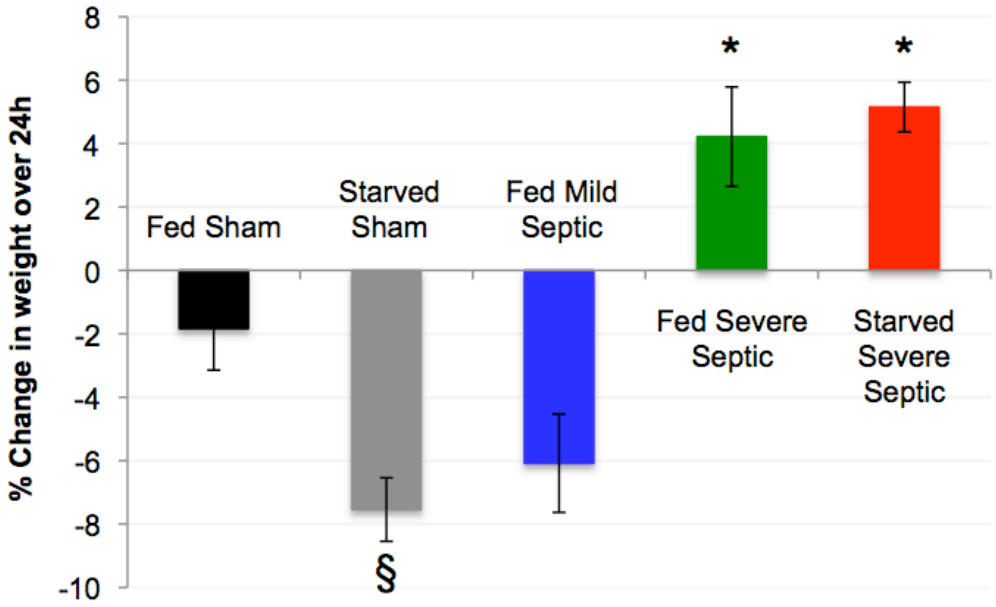


**Figure 2.8** Percentage change in body weight over 24 hours following i/p injection of faecal slurry or saline.

§ $p<0.05$ compared to fed sham and severe septic groups; *$p<0.05$ compared to fed sham, starved sham and mild septic (one way ANOVA).

### 2.3.3 Cardiac output and peak aortic blood flow velocity decrease in severe sepsis

Serial echocardiograms were performed at 0, 3, 6 and 24h to investigate cardiovascular responses to faecal peritonitis, and the adequacy of the subcutaneous fluid regimen. Sham animals required anaesthesia with 1.5-2% isoflurane, and severe septic mice only 0.5-1%.

Fifteen sham and thirty septic mice were evaluated. Of the 30 septic mice, eight developed mild sepsis, three moderate sepsis, and 13

severe sepsis. Six septic mice died before 24h. Demographic data were similar between groups (Table 2.5). A survival curve is shown in Fig 2.9.

| Group | Number | Age (weeks) | Weight (g) |
|---|---|---|---|
| Sham | 15 | 22.5 ± 0.7 | 31.3 ± 0.8 |
| Mild Septic | 8 | 20.9 ± 0.9 | 32.8 ± 1.0 |
| Severe Septic | 13 | 22.1 ± 0.7 | 30.9 ± 0.7 |
| Dead before 24h | 6 | 23.6 ± 1.2 | 33.8 ± 1.2 |

**Table 2.5** Demographic data of mice that underwent serial echocardiography over 24h. One way ANOVA showed no significance.

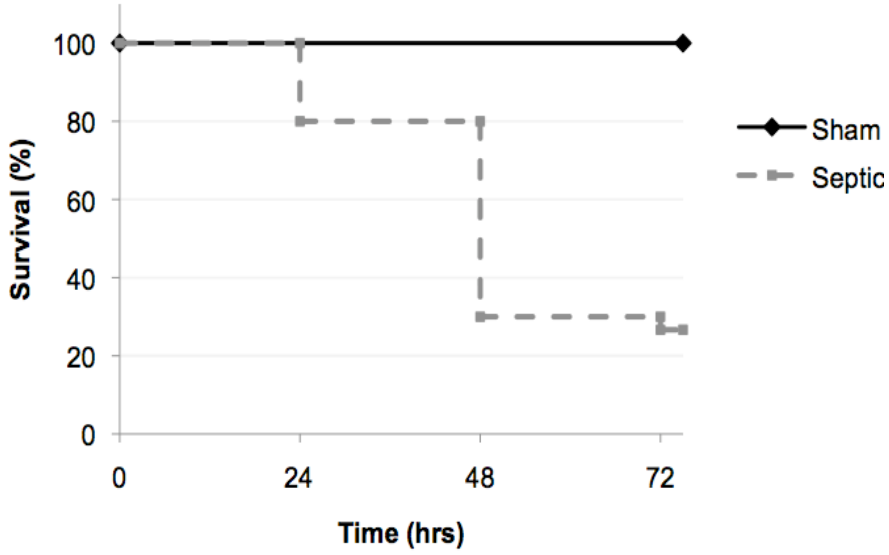


**Figure 2.9** Kaplan-Meier survival curve of septic mice undergoing serial echocardiography over 72 hours following injection of faecal slurry i/p.

Fig. 2.10 shows haemodynamic measurements in sham and septic mice. As early as 3h there were profound changes in stroke volume and peak velocity in severely septic animals. These changes were more pronounced by 6h with a smaller left ventricular cavity indicative of

hypovolaemia (videos taken at various time-points are on supplemental CD). Heart rate was initially maintained at 3 hours, but then progressively declined, following the trend in body temperature (Fig 2.7).

By 24 hours, the LV cavity size had returned to the original 0h size (see videos), but peak velocity remained low, implying poor myocardial contractility. Stroke volume had partially recovered and, in conjunction with the falling heart rate, resulted in poor cardiac output.

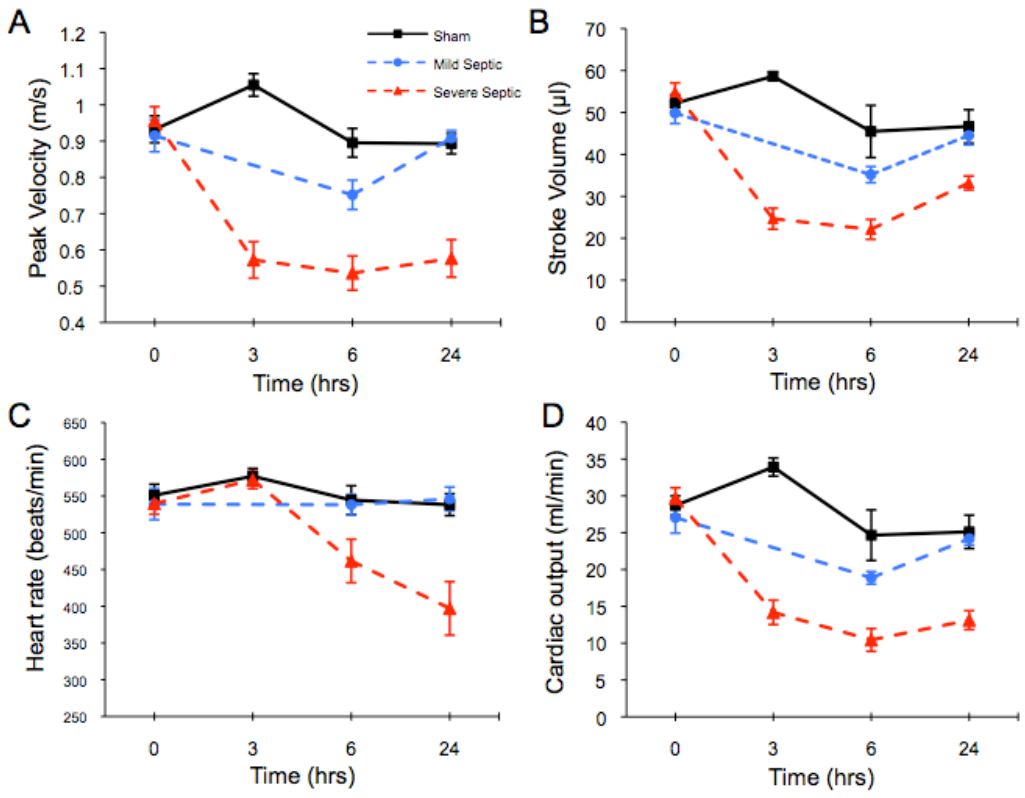


**Figure 2.10** Aortic peak velocity (A), stroke volume (B), heart rate (C) and cardiac output (D) of sham, mild septic and severe septic mice at 0, 3, 6 and 24h from i/p injection of faecal slurry or saline.

P<0.005 two way ANOVA with repeated measures comparing the severe septic group to the mild septic and sham groups.

#### 2.3.3.1 Cardiovascular response to intravenous fluid boluses in early severe sepsis is different to that seen in late severe sepsis.

The above results suggest that early cardiovascular changes in severe sepsis are due mainly to hypovolaemia, while later changes may be due to a high afterload and myocardial dysfunction. In order to define and quantify the septic myocardial dysfunction, fluid responsiveness of the cardiovascular system was tested at 6 and 24h.

Boluses of fluids were delivered via the internal jugular cannula while continuously measuring BP. Echocardiograms were performed immediately post-insertion of catheters (baseline), and after cumulative totals of 0.5, 1, 1.5, 2, 2.5 & 3 ml of hetastarch had been injected. To remove the effect of hypothermia on cardiovascular function, the mice were warmed gently during the operative period using a warming mattress. All echocardiograms were performed with core temperatures >34°C. Operative time was approximately 30 mins. Fluid losses during this time (evaporative losses from open wound) were not replaced.

Peak velocity, stroke volume and cardiac output of the severely septic mice were reduced at 6 and 24h compared to baseline values (Fig. 2.11). Peak velocity fell to 68 ± 4% of baseline at 6h, and 63 ± 5% at 24h ($p<0.05$ two-way ANOVA). Stroke volume fell to 54 ± 3% of baseline at 6h and 55 ± 6% at 24h ($p<0.05$). A non-significant rise in heart rate was noted at 6h but, at 24h, heart rate had fallen to 88 ± 6% of the baseline value ($p<0.05$, Wilcoxon signed-rank test). Cardiac output at 6h fell to 58 ± 4% of initial value, and to 48 ± 4% at 24h ($p<0.05$).

After two 0.5 ml fluid boluses, peak velocity, stroke volume and cardiac output increased in all groups ($p<0.05$) (Fig. 2.11). This was most marked in the 6h septic mice. A plateau was reached after 1.0 ml of fluid in all groups. No significant change was seen in heart rate of either sham or septic groups following the fluid boluses.

The cardiovascular response to fluid in the 6h septic mice was homogenous and similar to sham mice ($p>0.5$) (Figs 2.11-2.13). The response in 24h septic mice was less marked ($p<0.035$ vs. sham and 6h septic mice). After 1.5 ml of cumulative fluid, the cardiovascular response of the 24h septic mice was heterogenous. Some maintained cardiac output with further fluid boluses, but others developed severe cardiac failure and died shortly after. The right ventricle (a difficult structure to visualise in mice) became prominent and dilated in the short axis view of the sickest mice (Fig 2.14). By contrast, sham and 6h septic mice could accommodate 3 ml of fluid without any reduction in cardiac output.

Fig 2.15 shows changes in left ventricular end-diastolic and end-systolic internal diameters at 6 and 24 h. Fractional shortening (a marker of myocardial contractility) was calculated using these diameters. There was no significant difference in initial (0h) diameters for the three groups ($p=0.121$). Septic groups showed a reduction in both diameters at 6 and 24h ($p<0.05$, paired t-test), while sham mice diameters were unchanged. Following i/v boluses, end-systolic and end-diastolic diameters returned to their initial 0h values ($p<0.05$, repeated measures ANOVA). Fractional shortening increased at 6 and 24h in both septic groups ($p<0.05$, paired t-test); after injection of IV fluid, this returned to initial 0h values.

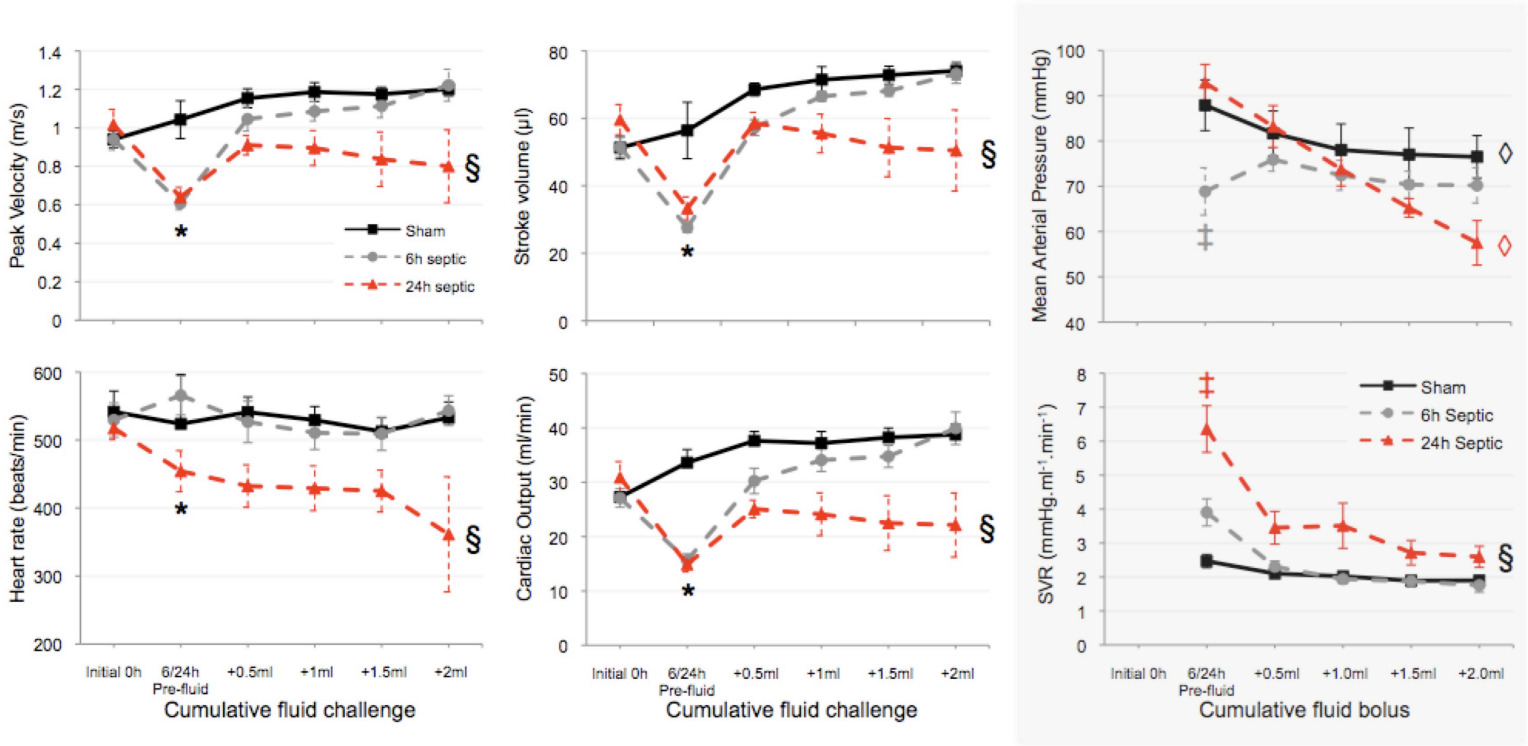


**Figure 2.11** Cardiovascular response of severe septic and sham mice measured at 0h and 6h or 24h time-points when fluid boluses of 0.5ml up to 2.0ml were administered to measure response to fluid challenge. * $p<0.05$ two-way RM-ANOVA comparing the 0h echo to the 6h and 24h echos. § $p<0.05$ for fluid challenge data comparing 24h septic mice and sham/6h septic mice. ‡ $p<0.05$ One-way ANOVA comparing the pre-fluid values. ◊ $p<0.05$ two-way ANOVA comparing within group data points.

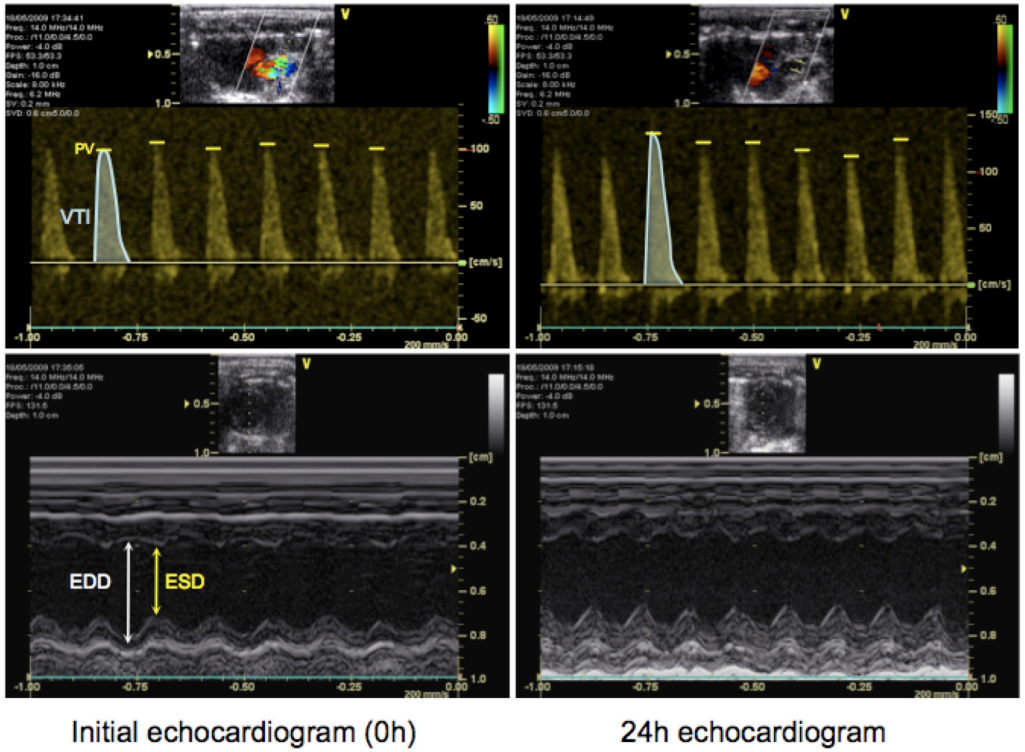


**Figure 2.12** Velocity-time integral (VTI) envelopes (top row) and M-mode images through the left ventricle at the papillary muscle level (bottom row) of sham mice at 0h and 24h. Peak velocities are marked by yellow horizontal bars. For each time-point, the stroke distance and peak velocity were the average of 6 envelopes and peaks. The M-mode images were used to measure end-systolic diameter (ESD), end-diastolic diameter (EDD), and calculate the fractional shortening.

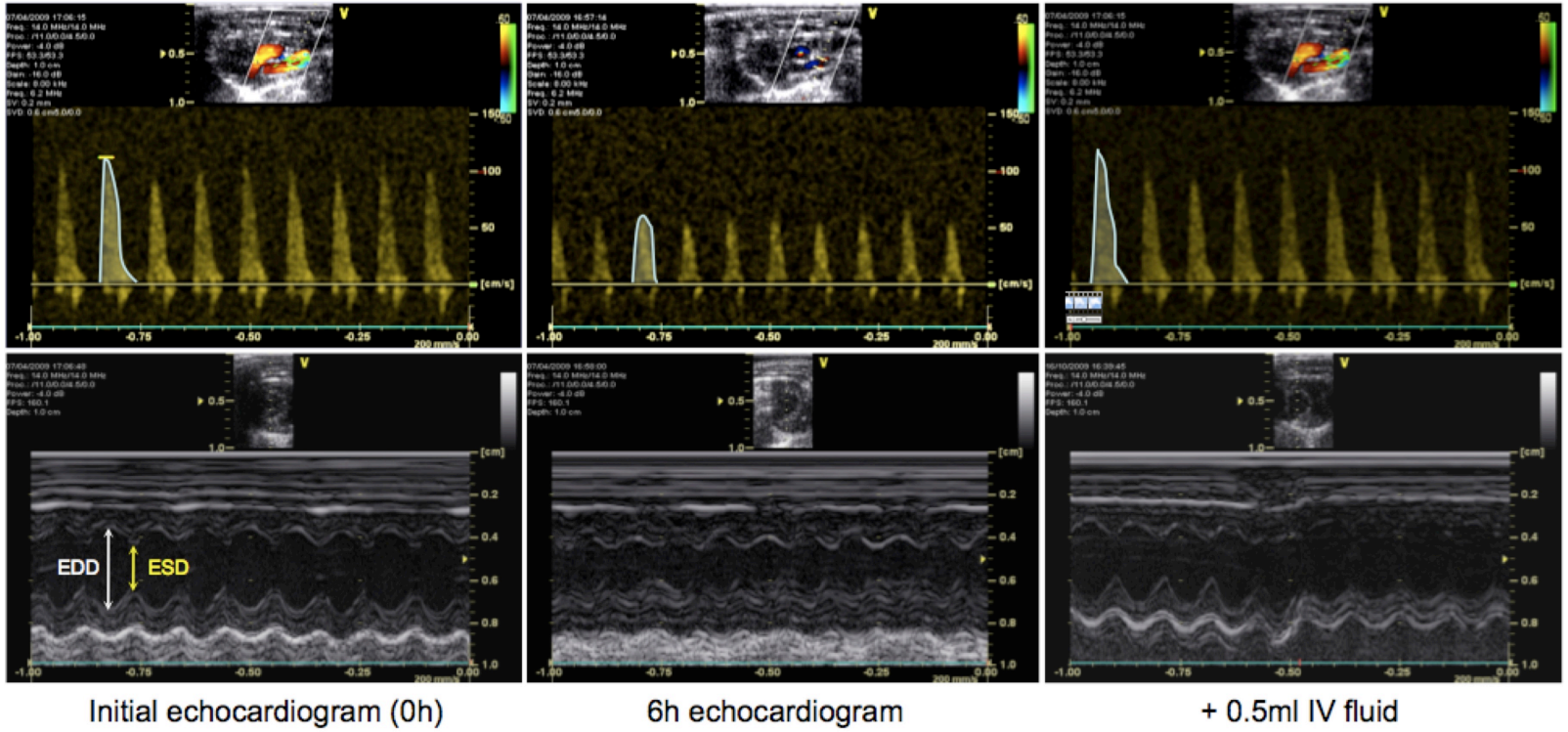


**Figure 2.13** Velocity time integral (VTI) envelopes outlined by blue line (top row), and M-mode images through the left ventricle at papillary muscle level (bottom row) of severely septic mice at 0h, 6h and at 6h following the first 0.5ml of fluid bolus. Intravenous fluid administration restores the VTI envelopes, as well as the end-systolic (ESD) and end-diastolic diameters (EDD).

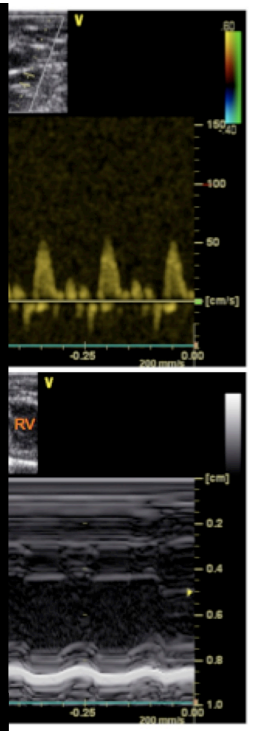


colloid

septic mouse at 24h.

The short-axis image

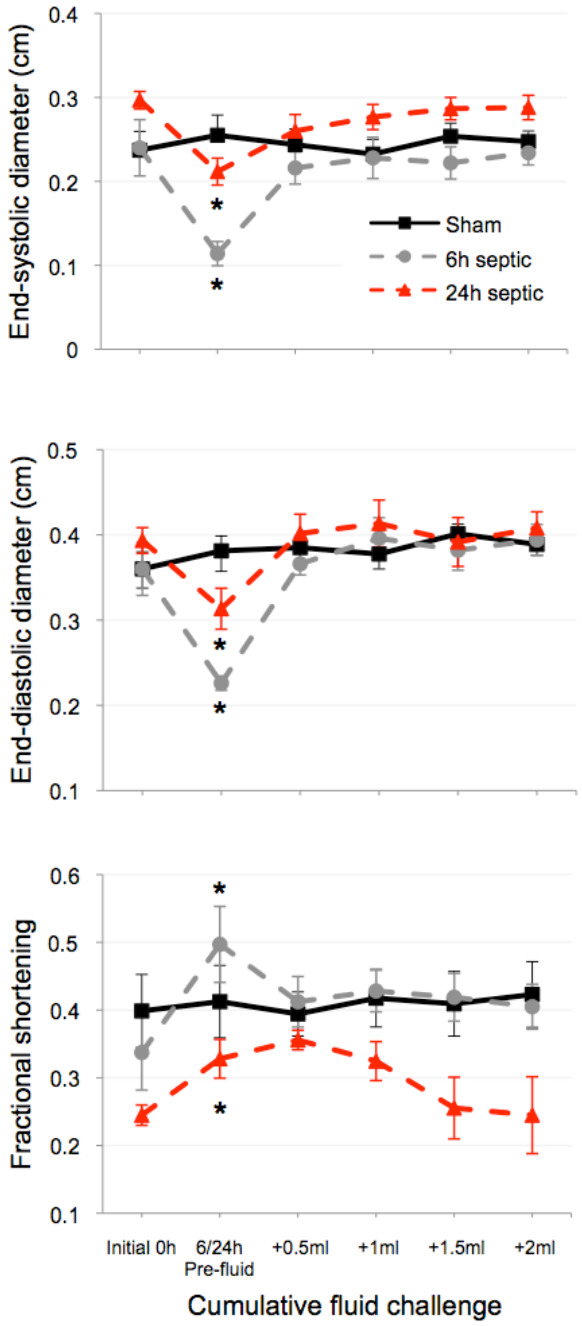


**Figure 2.15** Changes in end-systolic and end-diastolic diameters, and fractional shortening of sham and severe septic mice before and after fluid boluses. Echocardiograms were performed at 0h, and repeated at 6h or 24h following vascular cannulation and injection of fluid boluses.

* $p<0.05$ paired sample t-test comparing 0h to 6 and 24h in the septic groups.

### 2.3.4 Oxygen consumption ($VO_2$) and carbon dioxide production ($VCO_2$) in healthy fed and starved mice.

Initial metabolic cage experiments were performed to obtain the metabolic rate in normal healthy mice, and to observe the impact of starvation. The mice adapted to their new environment in the metabolic cages within 2-3 hours. Therefore, all recordings were made after this period of acclimatisation. Fig 2.16 shows total body oxygen consumption ($VO_2$) of two mice aged 22 weeks. Diurnal variation in metabolic rate reflected nocturnal habits of rodents with increased $VO_2$ and more frequent spikes of activity at night-time.

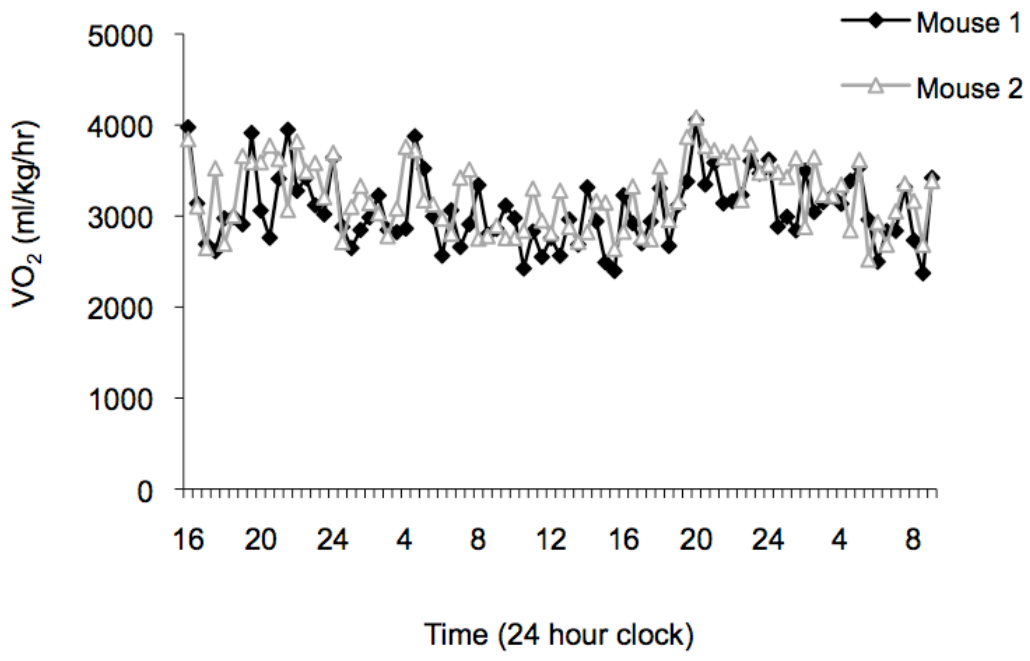


**Figure 2.16** Total body oxygen consumption of two C57 black mice under standard conditions, with free access to food and water. Three hours of acclimatisation was allowed prior to start of recordings. Each datapoint is the average of 4 recordings (8 mins apart) over 30 mins.

### 2.3.4.1 Metabolic rate, temperature and weight in starvation

The effect of starvation on total body metabolism was observed in two separate experiments. In the first, six mice were placed into separate metabolic cages and, after an initial 4h period of acclimatisation, food was withdrawn but water was freely available. $VO_2$ and $VCO_2$ were measured over time. Food was re-introduced after 20 hours of starvation.

Figure 2.17 shows that as starvation commenced, the $VO_2$ dropped to a nadir of 55 ± 5% of pre-starvation values at 10h ($p=0.002$) and remained low thereafter (67 ± 5% of baseline at 20h; $p=0.021$). $VCO_2$ followed the same pattern; being 50 ± 5% and 60 ± 5% of the starting values at 10h and 20h, respectively ($p=0.005$). Following re-introduction of food, $VO_2$ and $VCO_2$ increased significantly. The respiratory exchange ratio (RER) indicated a mix of fuel usage (RER=0.85) during the initial acclimatisation (Fig. 2.17). With the onset of starvation, RER dropped to 0.72 ± 0.02 at 10h ($p=0.032$), implying a switch to predominantly fatty acid oxidation. Upon re-feeding, the ratio increased rapidly to 0.95 ± 0.03 within 2h ($p=0.000$), indicating a switch back to carbohydrate metabolism.

Despite the drop in metabolic rate with starvation, core temperature remained unchanged (Fig 2.18A). Body weight dropped by 10% over the 24-hour period (from 28.5 ± 0.9g to 25.4 ± 0.8g at 20h; $p<0.05$) [Fig 2.18B].

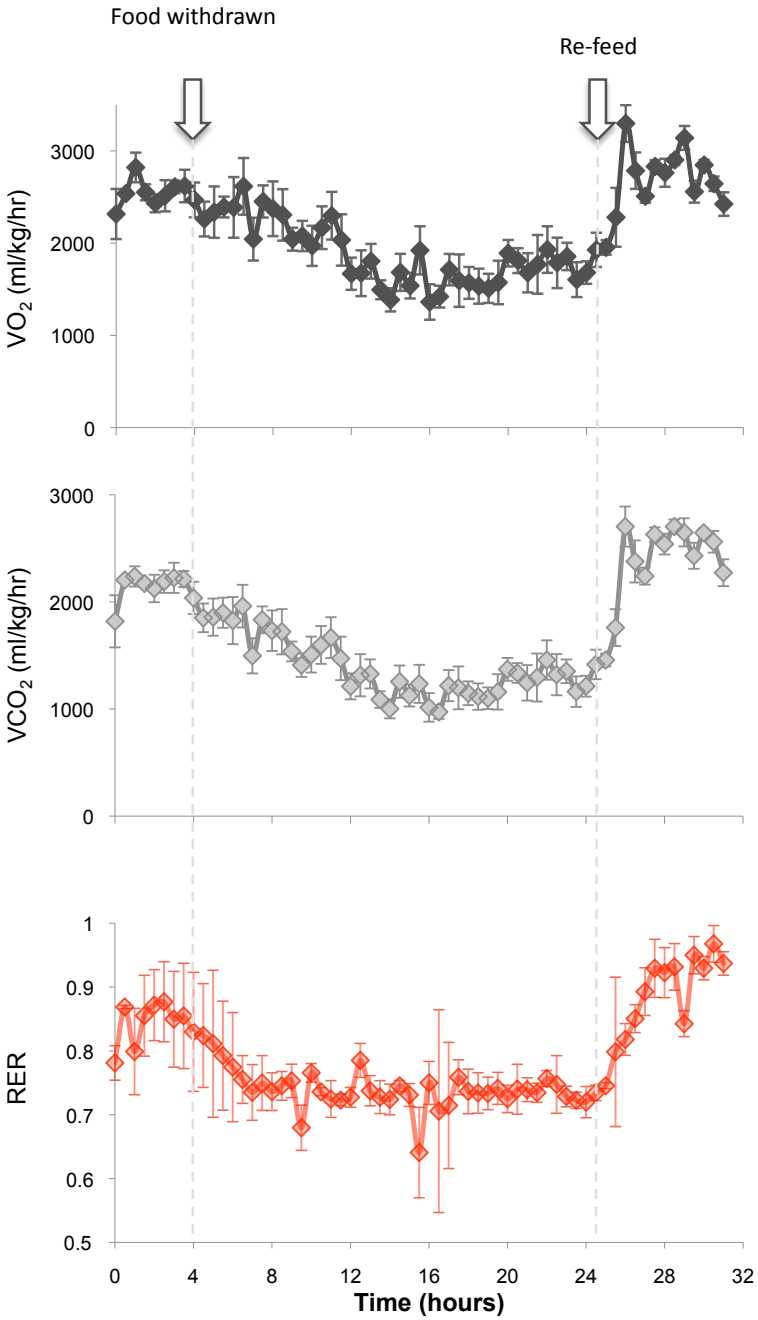


**Figure 2.17** Effect of starvation on $VO_2$, $VCO_2$ and respiratory exchange ratio (RER) in 6 healthy naïve mice. A 4-hour period of acclimatisation was allowed prior to withdrawal of food. Error bars represent SEM.

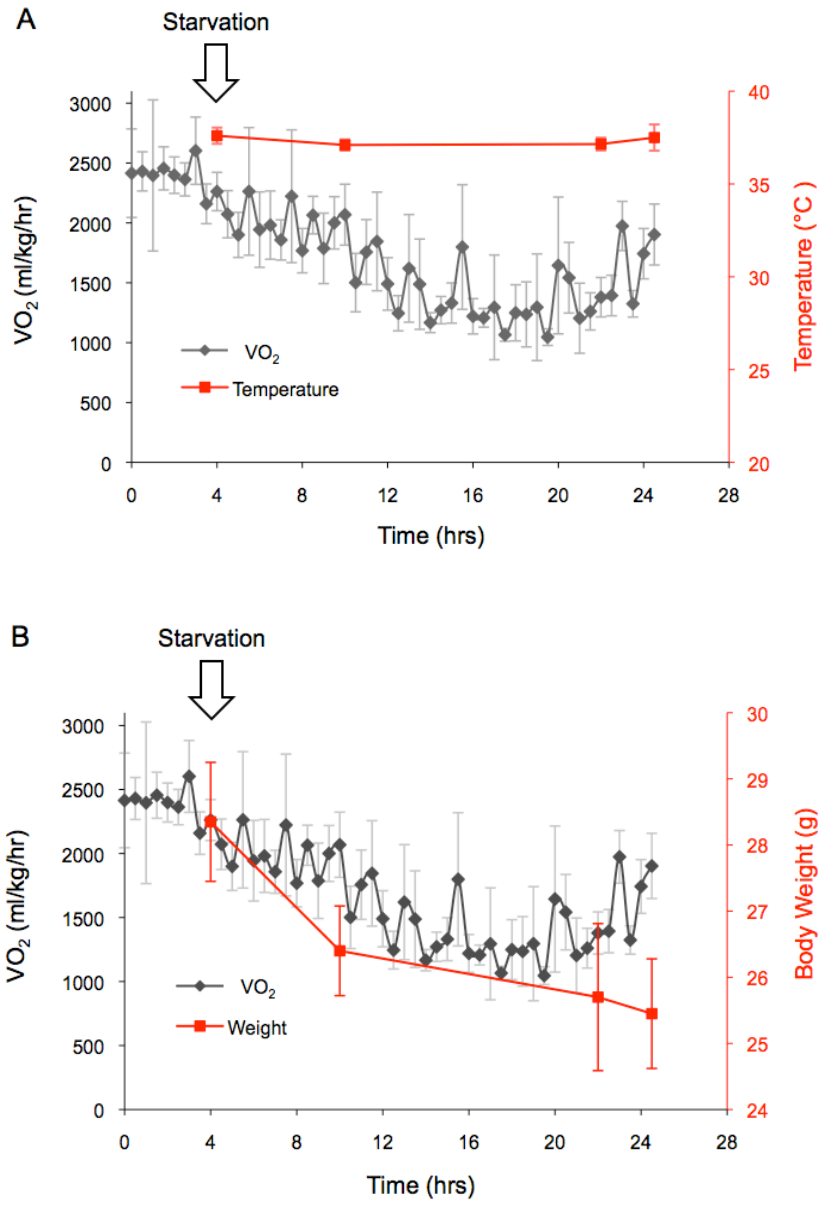


**Figure 2.18** Change in $VO_2$ with starvation plotted alongside core temperature (A) and body weight (B). Error bars=SEM. (n=4 animals)

The *second* of these experiments investigated the effect of subcutaneous fluid given at 6h and 18h time-points on $VO_2$, $VCO_2$ and RER in sham fed and starved animals. The fluid boluses consisted of 5% dextrose in 0.81% saline and resulted in a short-lived (1.5 h) increase in $VO_2$, $VCO_2$ and RER in the starved mice, but no effect in the fed mice.

### 2.3.5 Whole body metabolic rate is reduced with severe sepsis

Total body metabolism was measured after i/p faecal slurry or 0.9% saline (sham). All mice received the standard fluid therapy regimen (saline 0.81%/ glucose 5%) at 0, 6 and 18h time-points. Mice were acclimatised in their metabolic cages for 3 h. All experiments were started at the same time of day to avoid bias due to diurnal variation in metabolic rate. Mice were allowed to recover for 1 h in a warm chamber prior to returning to their cages to the start of recordings.

Six mice were in each sham group (fed or starved) and 13 in the septic group (all starved). Six developed mild sepsis and 7 became severely affected. Following induction of sepsis, there were early reductions in $VO_2$ and $VCO_2$ (Fig. 2.19), that increased in magnitude with disease severity (Table 2.6). The $VO_2$ of severe septic mice reached a nadir of 468 ± 40 ml/kg/hr at 24h (20% of starting $VO_2$; $p<0.05$). All these mice died within the next few hours. Interestingly, even at the 1h time-point, the $VO_2$ was significantly lower in the septic mice (Table 2.6).

Similar reductions (and diurnal variation) in metabolic rate were seen in the mild septic and starved sham mice (Fig 2.19). The $VO_2$ of the mildly septic mice returned to baseline values after 16 h. This coincided with normalisation of temperature and an increased level of alertness and activity. However, RER remained between 0.7-0.8 as they were still starved. The RER in the starved sham and severe septic groups also remained between 0.7-0.8 throughout the 24h experimental period. In contrast, RER in sham fed mice was >0.9 from 6h onwards (Fig 2.19C).

A further feature in the septic mice was the loss of variability in $VO_2$ and $VCO_2$ compared to the sham animals (Fig 2.20). The sham mice characteristically displayed multiple spikes over a 1-hour period, whereas the septic mice lost their spike activity 3-4 hours post-injection of slurry. This was seen in both mild and severely septic mice, although some $VO_2$ spiking returned in the mildly septic mice after 12h.

| Group | 1h $VO_2$ (ml/kg/hr) | 5h $VO_2$ (ml/kg/hr) | 10h $VO_2$ (ml/kg/hr) | 15h $VO_2$ (ml/kg/hr) | 20h $VO_2$ (ml/kg/hr) |
|---|---|---|---|---|---|
| Fed Sham | 3025 ± 156 | 2873 ± 337 | 2847 ± 178 | 2985 ± 282 | 2424 ± 152 |
| Starved Sham **§** | 3036 ± 138 | 1799 ± 150 | 2213 ± 91 | 2007 ± 271 | 1844 ± 146 |
| Mild Septic **§** | 2619 ± 139 **‡** | 1829 ± 157 | 2091 ± 372 | 2038 ± 322 | 2494 ± 100 |
| Severe Septic * | 2341 ± 244 **‡** | 1045 ± 293 | 827 ± 146 | 720 ± 146 | 550 ± 87 |

**Table 2.6** Whole body oxygen consumption ($VO_2$) of sham and septic mice at 1, 5, 10, 15 and 20h post i/p saline (sham) or faecal slurry (septic). Values denote mean ± SEM. * p=0.000 two-way RM-ANOVA comparing severe septic group against all other groups. **§** p<0.04 two-way RM-ANOVA comparing starved sham and mild septic series vs. fed sham and severe septic. **‡** p<0.05 significance when the 1h data of the septic animals is compared to the sham groups by ANOVA.

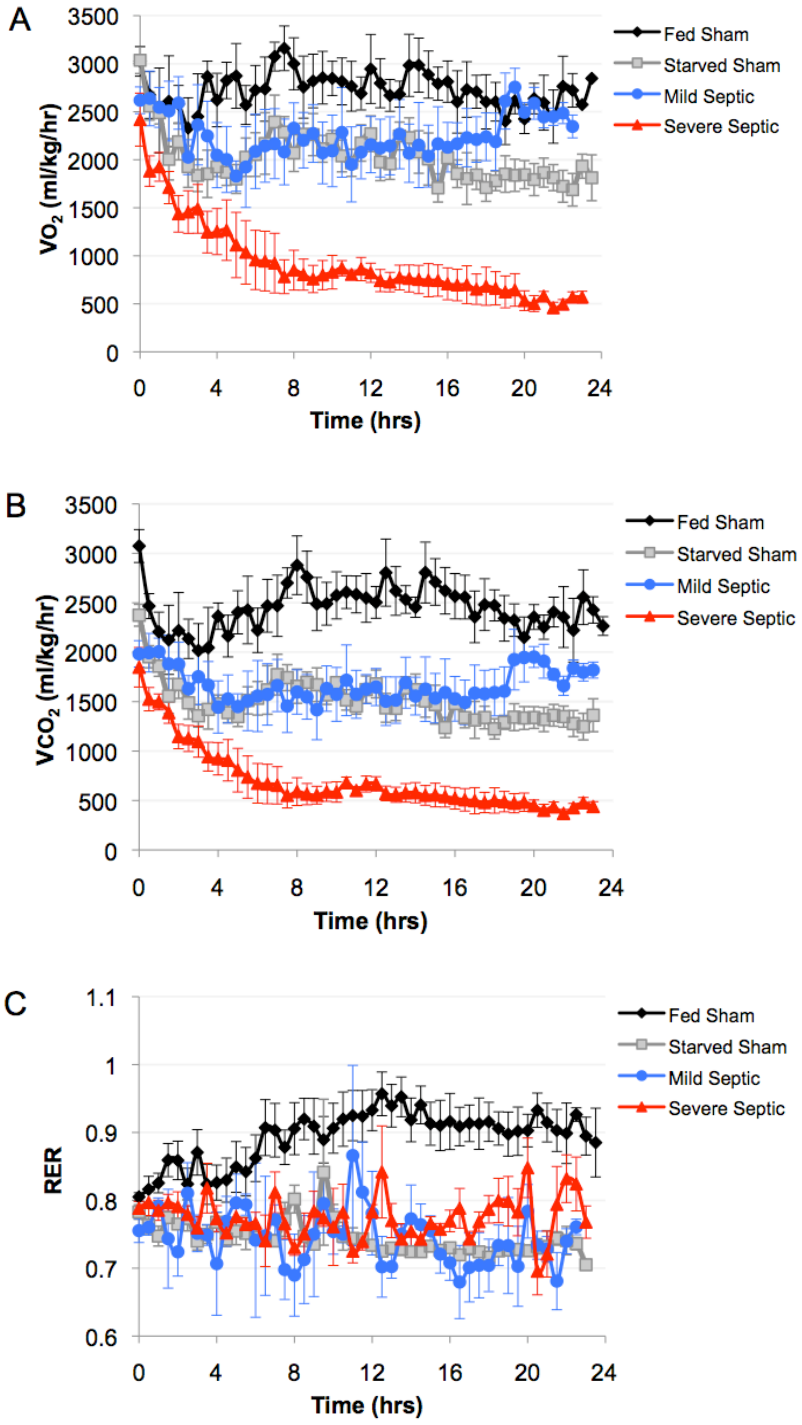


**Figure 2.19** $VO_2$ (A), $VCO_2$ (B) and RER (C) of sham and septic mice. 0h signifies the start of recordings 1-hour post injection of faecal slurry. Error bars = SEM. $P<0.05$ two-way RM-ANOVA comparing $VO_2$ & $VCO_2$ of severe septic vs. other groups, and when comparing starved sham and mild septic with the fed sham group.

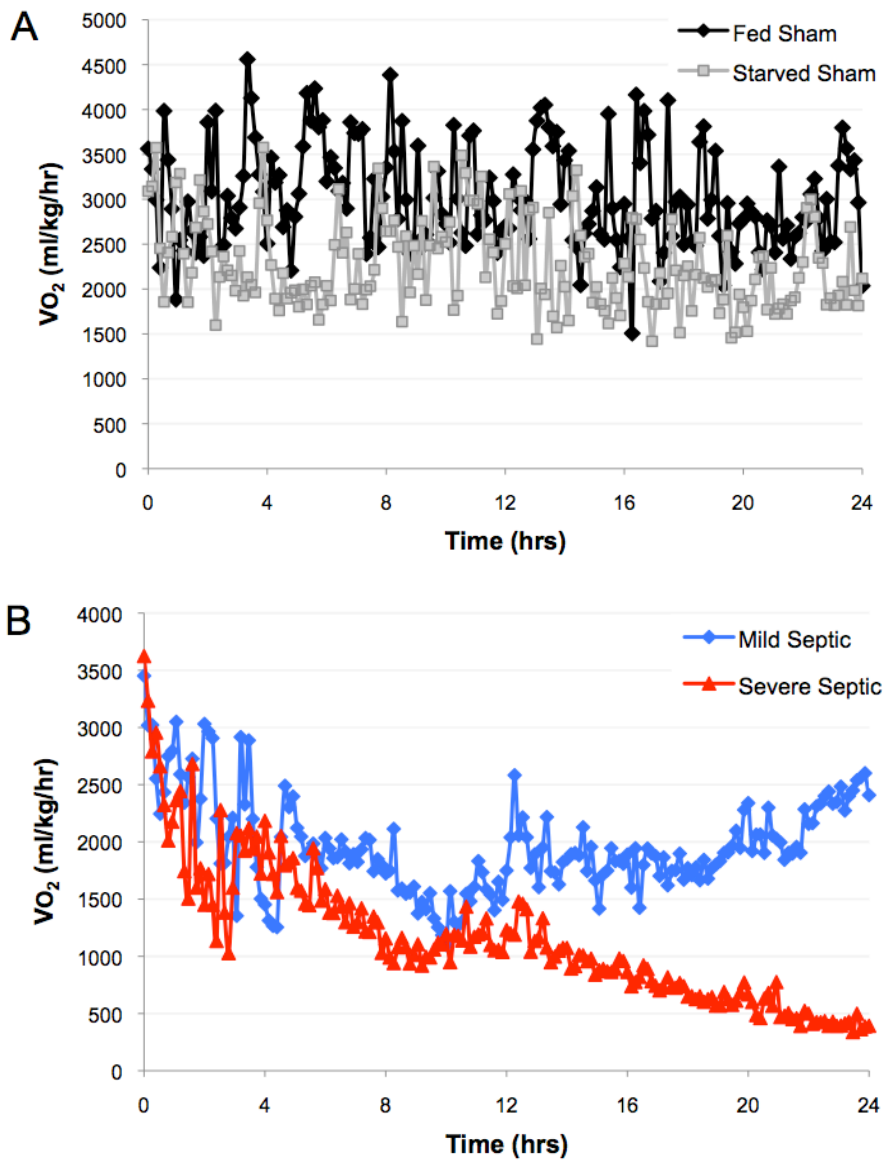


**Figure 2.20** Trace of $VO_2$ of a fed and a starved sham mouse (A), and a mild septic and a severely septic mouse (B) over a period of 24 h. The individual points are $VO_2$ values taken at 8 min intervals. Sham animals display a high degree of variability between successive readings, whereas septic animals lose this variability within a few hours after induction of sepsis.

### 2.3.5.1 Relationship between temperature and $VO_2$

As the $VO_2$ of severely septic mice fell, so did their core temperature (Fig 2.21). This is in contrast to starved sham mice where, despite a reduction in $VO_2$ with starvation, no significant change in core temperature was seen (Fig 2.18A). Fig 2.22 summarises this finding in a plot of the $VO_2$ against temperatures of septic and starved sham mice.

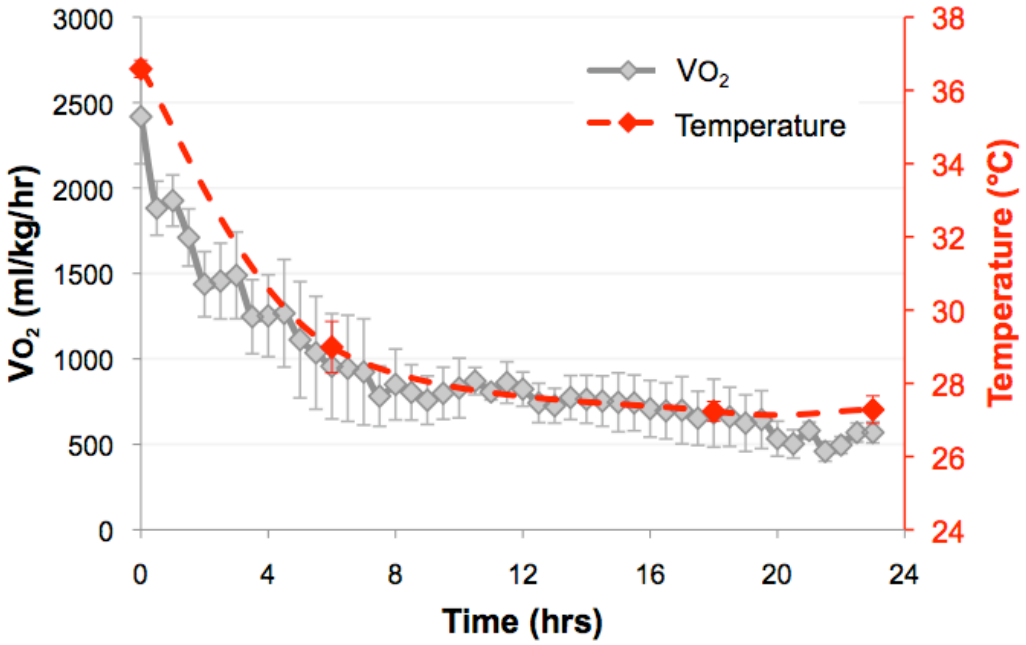


**Figure 2.21** $VO_2$ and core temperature of mice after i/p injection of faecal slurry at time 0h (n=7). The mice displayed clinical signs of severe sepsis (scores of 5+). Core temperatures were measured at 0, 6, 18 and 24h.

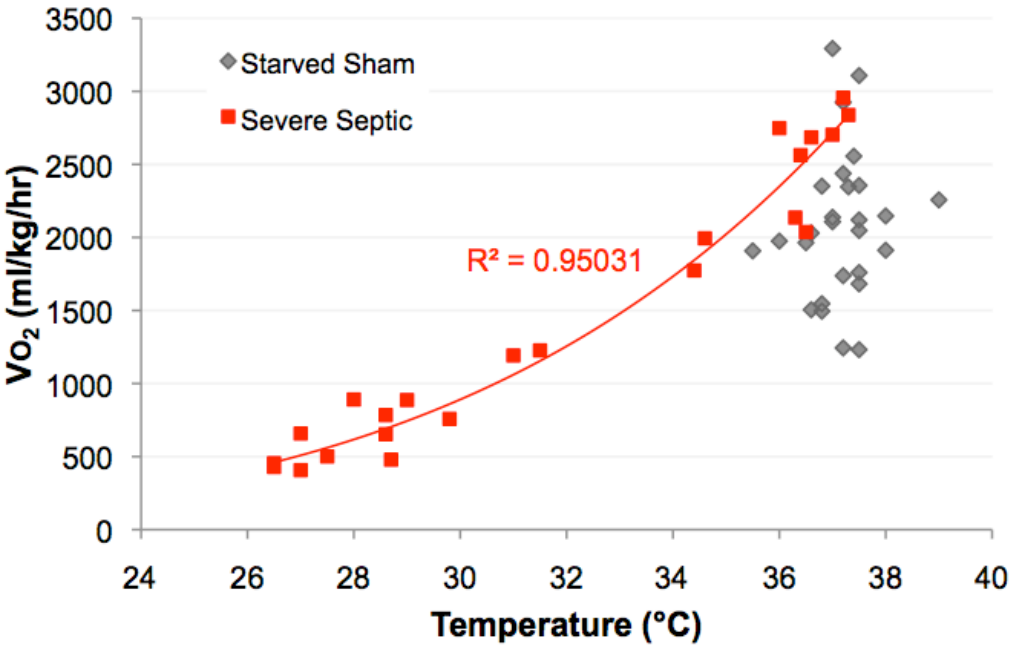


**Figure 2.22** Temperatures of starved sham (grey points) and severe septic (red points) mice taken at different time-points and plotted against their corresponding $VO_2$ values. A curve of best fit has been drawn through the severe septic data. In the severe sepsis group, the points are generally concentrated at the top right of the graph at the beginning of the experiment (i.e. 0h and 6h) and shift to the bottom left with progression and worsening of the disease process (i.e. 18h and 24h).

### 2.3.5.2 Effect of re-warming on $VO_2$ and cardiac output in severe septic mice

These studies were performed to investigate whether the reduction in $VO_2$ in severe septic mice was due to hypothermia. Six severe septic mice were injected with i/p faecal slurry with five developing severe sepsis. They were re-warmed to 37°C at 10h and 24h time-points and

$VO_2$ re-measured. All five mice survived to the 10h time-point but only three survived to 24h; a further mouse died during the re-warming process at 24h. Core temperatures were recorded before and after re-warming, and prior to transfer back to their metabolic cages. Trans-thoracic echocardiography was performed on three of the six mice at baseline (0h), pre-warming and post-warming at 10h and 24h time-points.

Core temperatures reached a low of 29.8 ± 1.1°C at 10h, and 29.5 ± 1.3°C at 24h. Following 1.5 h of re-warming, temperatures increased to 37.1 ± 1.2°C at 11.5h, and 36.7 ± 2.4°C at 25.5h [$p<0.05$] (Fig 2.23). Restoration of normal body temperature only led to a modest rise in $VO_2$ (from 925 ± 131 to 1190 ± 131 ml/kg/hr at 10h [$p=0.007$]; and from 730 ± 90 to 941 ± 178 ml/kg/hr at 24h; [NS]). This modest rise occurred despite a 2-fold increase in cardiac output (from 9.7 ± 2.0 to 19.1 ± 2.7 ml/min post-warming at 10h [$p=0.002$], and from 15.8 ± 1.4 to 32.3 ± 9.2 ml/min after warming at 24h [NS]). Statistical significance was not reached at the 24h time-point as only two mice survived to this stage.

Once back in their metabolic cages, core temperature and $VO_2$ fell rapidly back to pre-warming levels within 1.5 h (to 31.7 ± 1.4°C and 956 ± 160 ml/kg/hr after the 10h re-warming episode; and to 29.4 ± 0.2°C and 699 ±1 ml/kg/hr after the 24h re-warming episode).

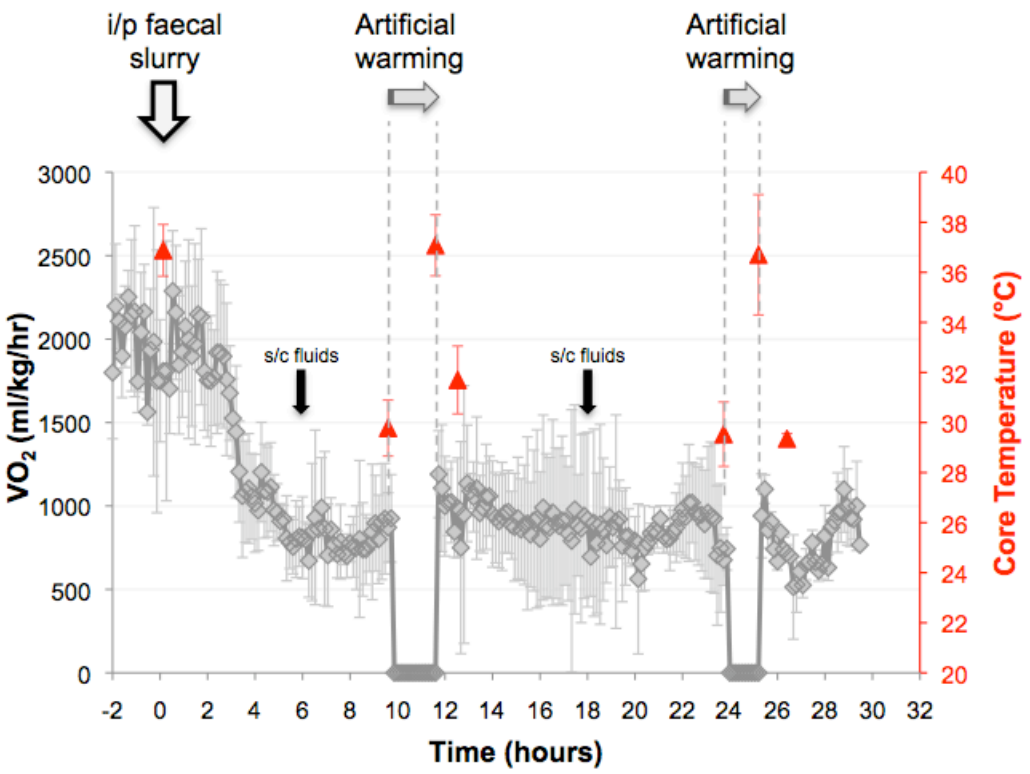


**Figure 2.23.** $VO_2$ and core temperature of mice with severe sepsis undergoing two episodes of warming over a 1.5 h time period (marked by the dashed lines). Mice were treated with s/c fluid boluses at 6 and 18h time-points. (Error bars are standard deviation).

Table 2.7 and Fig. 2.24 summarize echo data. As shown before, peak velocity and stroke volume fell in line with temperature and metabolic rate at 10h and 24h. Cardiac output was reduced to one-third of baseline at 10h, and to half baseline at 24h ($p<0.05$).

Following re-warming, there was a two-fold improvement in cardiac output. As sample size is small, these results should be treated with some caution however, even with three mice per group, the results

reached statistical significance at 10h, implying that hypothermia in severe sepsis has a profound effect on cardiovascular performance.

| | Baseline | 10h re-warming | | 24h re-warming | |
|---|---|---|---|---|---|
| | | Pre | Post | Pre | Post |
| **Temperature (°C)** | 36.1 ± 0.2 | 30.0 ± 1.5 § | 36.3 ± 0.6 * | 28.8 ± 2.1 § | 36.6 ± 1.7 |
| **$VO_2$ (ml/kg/hr)** | 2288 ± 181 | 925 ± 131 § | 1190 ± 131 * | 730 ± 90 § | 941 ± 178 |
| **Peak velocity (m/s)** | 1.06 ± 0.06 | 0.46 ± 0.08 § | 0.80 ± 0.10 * | 0.66 ± 0.07 § | 1.14 ± 0.13 |
| **Heart rate (beats/min)** | 509 ± 31 | 452 ± 23 | 601 ± 45 * | 435 ± 6 | 614 ± 47 |
| **Stroke volume (µl)** | 60 ± 3 | 21 ± 3 § | 32 ± 6 * | 36 ± 4 § | 52 ± 11 |

**Table 2.7** Temperature and echocardiography data from severe septic mice at baseline (0h), and pre- and post warming at 10h and 24h. Warming took place over 1.5 hours. Mice were only anaesthetized for the period of echocardiography. Values denote mean ± standard deviation.

* $p<0.05$ paired t-test comparing post-warming values to their corresponding pre-warming value. § $p<0.05$ paired t-test comparing the values to corresponding baseline (0h) values.

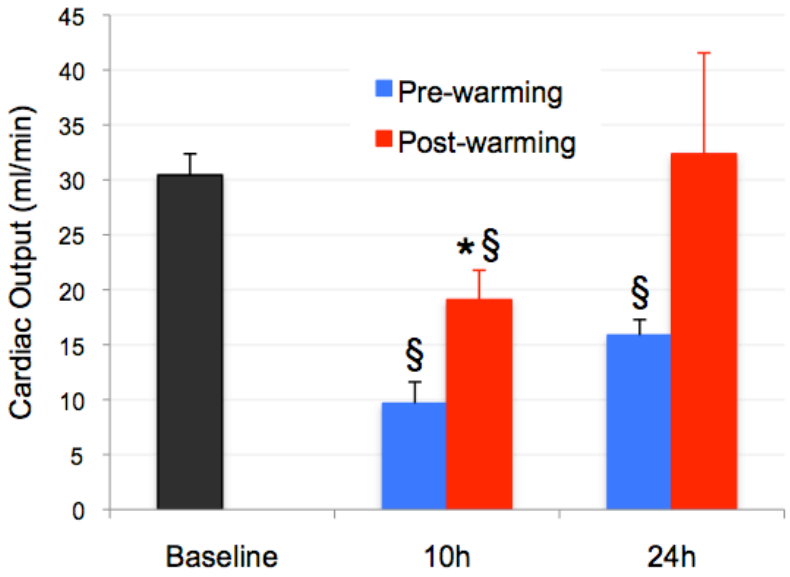


**Figure 2.24** Cardiac output at baseline (0h), pre-warming and post warming at 10h and 24h time-points. There was a two-fold increase in cardiac output following warming at the two time-points.

* p<0.05 paired t-test comparing post-warming to pre-warming values.

§ p<0.05 paired t-test comparing values to baseline values.

## 2.4. Discussion

### 2.4.1 Animal model of sepsis and *in-vivo* findings

Mice are frequently used for lab models of sepsis because of their ready availability, relatively low costs and the ability to knock-in or knock-out specific genes. In order to use animal models to understand disease

processes and to trial therapeutic options, it is vital to understand how the model behaves and whether or not it resembles the human form sepsis.

I found the initial mouse model did not meet my requirements as instrumentation and connection to the tether system then in use was detrimental to their wellbeing. Indeed, only 67% of sham treated mice lived to 48h. Also as the intra-arterial line became obstructed frequently, I decided to simplify the model by no longer inserting vascular lines, and instead giving subcutaneous resuscitation fluid 6-12 hourly. To improve reproducibility, faecal slurry was injected i/p. under direct vision.

I expended considerable effort in attempting to standardize the septic insult without the need for regular microbiological support (culturing and quantifying bacteria), and to achieve the severity of illness necessary for the experiments at the various time-points studied. I also tested different subcutaneous fluid resuscitation regimens, as previously described (Hollenberg, Dumasius et al. 2001; Miyaji, Hu et al. 2003). It was clearly important that the mice should develop organ failure as a result of sepsis yet, at the same time, avoiding cardiovascular collapse due to hypovolaemia caused by increased capillary leak and decreased fluid intake. Serum biochemistry demonstrated organ dysfunction in the severely ill animals while the sham and mild septic animals maintained normal vital organ function, at least within the parameters of the tests performed.

Each mouse received 4 ml of fluid s/c over the 24h period. This is equivalent to twice their circulating volume (75ml/kg) and comparable to clinical practice in human sepsis where large volumes of fluids are

required in the first 24-48 hours after the onset of sepsis (Rivers, Nguyen et al. 2001).

This model generated a 100% sham animal survival and a divergent septic population. The host lab's established clinical scoring system for rats was adopted for assessing sepsis severity in mice. This was found to be robust and correlated well with the biochemical markers of organ dysfunction where incremental rises were seen in serum urea, creatinine and liver function tests with increasing severity. The scoring system also correlated well with the blood gas data. Severely ill mice had a significantly lower blood pH that was of a mixed respiratory and metabolic nature. High arterial $pCO_2$ values were likely to be as a result of lower lung compliance, respiratory muscle fatigue, heart failure (see later), and hypothermia affecting respiratory centre activity. As part of the inflammatory reaction, the diaphragm muscle of severely septic mice has been shown to generate less force than their naïve/sham counterparts with earlier fatigue (shown later in this thesis and (Supinski, Nethery et al. 1996)). Furthermore, the pleural cavities of the severely septic mice were consistently found to be filled with straw-coloured effusion and their abdomen filled with pus and dilated loops of bowel. All of these findings are known to hinder diaphragmatic excursion and can lead to respiratory failure with a rising arterial $pCO_2$. Despite this rise in arterial $pCO_2$ and the likelihood of acute lung injury, no significant change was observed in arterial $pO_2$. This (or even an increase) is also seen in rat models of shock and metabolic acidosis established within the lab, and implies that rodent lung physiology varies to some extent from the human response.

I was surprised to note acidaemia in the naïve and starved sham mice (base deficit of 7.7 ± 2.6 and 8.8 ± 0.7 mmol/l, respectively). These values are clearly higher than normal values of ±2 mmol/l seen in healthy humans and rats. The plasma bicarbonate levels were also low in the naïve and sham mice (18 ± 2 mmol/l), albeit these value are derived from the pH and $PCO_2$ data. Other groups have also reported these findings in C57bl/6J mice (Henriksnäs, Phillipson et al. 2005; Sjöblom and Nylander 2007). As metabolic acidosis was significantly worse in the severely septic mice (base deficit of 18.8 ± 3.3 mmol/l), I did not pursue this further. Similarly, I was surprised to note raised serum lactate levels in the healthy animals (e.g. 5.6 ± 0.4 mmol/l in the naïve mice) that did not increase markedly in the septic animals. Again, other researchers have reported similar elevations in healthy mice (Lewis, Haase et al. 2001; Hakimi, Yang et al. 2007), though others have noted values similar to normal humans and rats (Kao, Xenocostas et al. 2007; Kruse, Watt et al. 2008). I re-tested the blood samples on an i-STAT® device (Abbott Labs, Chicago, IL, USA) and after obtaining similar results, decided not to use blood lactate as a marker of sepsis severity.

Starvation had a profound effect on the body weight (7.7% reduction; $p<0.05$). This is likely to be mainly as a result of reduction in the fat stores, which have been shown to drop by one-third in a 14 hour non-feeding period (Bronson 1987). Septic mice in this model, exhibited a change in behaviour with a reduction in movement and anorexia. This was seen even in the mildly sick mice resulting in a significant weight loss from baseline levels (6.2% reduction; $p<0.05$). These behavioural

changes were more pronounced in severely ill animals, however, these mice gained weight (5% gain; $p<0.05$), most likely due to reduced s/c fluid absorption, reduced fluid clearance due to renal dysfunction, increased capillary leak, pleural/ascitic fluid and pus, and dilated fluid-filled loops of bowel.

Only 10% of septic patients present with hypothermia (<35°C) (Clemmer, Fisher et al. 1992; Peres Bota, Lopes Ferreira et al. 2004). Interestingly, hypothermia is an independent predictor of mortality in sepsis (Arons, Wheeler et al. 1999; Peres Bota, Lopes Ferreira et al. 2004). In my study, the septic mice became hypothermic and this was more profound in the severely ill animals. Other groups reported similar findings; for instance, (Yu, Barger et al. 2000) reported that core temperature in endotoxaemic mice fell to 30°C at 8h accompanied by a two-thirds reduction in basal metabolic rate. I too found an early fall in temperature occurring within a few hours of induction of sepsis that also correlated with the reduction in $VO_2$. Even mildly septic mice exhibited a small decrease in core temperature by 6h, though this recovered by 18h. However, the severely ill animals remained hypothermic until 24h when the study was terminated. This hypothermic response was unrelated to the anorexic effect of sepsis as naïve fasting animals did not become hypothermic, although they did show a significant decrease in $VO_2$ that was limited and normalized upon re-feeding.

In the severely ill mice, a close correlation was found between $VO_2$ and body temperature. Thus, was the drop in temperature due to the fall in $VO_2$, or *vice versa*? To answer these questions, the severely septic

animals were artificially warmed to 37°C at 10h and 24h. Despite an almost two-fold rise in cardiac output and hence oxygen delivery, there was only a small rise in $VO_2$. These results imply that temperature had little effect on $VO_2$ in severely septic mice, although it clearly influences cardiovascular function.

Total daily energy expenditure is divided into resting metabolic rate (60-75%), diet-induced thermogenesis (10-15%) and the remainder as activity-related thermogenesis (Donahoo, Levine et al. 2004). There are additional effects on total energy expenditure in critically ill people related to the illness itself as a result of high levels of catecholamines and other stress hormones, as well as development of fever, agitation and increased respiratory workload (Chioléro, Revelly et al. 1997). Treatment strategies can also influence energy expenditure, so that sedative drugs and mechanical ventilation lead to a reduction and catecholamine infusions lead to an increase in total energy expenditure.

Most human studies show maintained or slightly increased (approximately 15%) resting energy expenditure in severe sepsis (Kreymann, Grosser et al. 1993; Frankenfield, Wiles et al. 1994; Chioléro, Revelly et al. 1997) with extensive protein and fat catabolism, negative nitrogen balance and hyperglycaemia. Importantly, a negative correlation is seen with sepsis severity (Kreymann, Grosser et al. 1993). Healthy human volunteers given endotoxin showed a 2°C rise in temperature, a 70% rise in oxygen delivery and a 40% rise in oxygen consumption after 4h (Soop, Albert et al. 2004). By contrast, in my mouse model, metabolic

rate was consistently reduced within 4 h of sepsis and remained low in the severely sick animals. Together with the core temperature response, this represents an important species difference between mice and humans. This may represent an adaptive shutdown to an extrinsic insult akin to hibernation, or a direct pathological effect of systemic inflammation on metabolic processes and/or mitochondrial energy supply (Singer, De Santis et al. 2004; Levy 2007). Notably, this hypothermic response is not shared with rats who become pyrexic when septic, provided they receive adequate fluid (Brooks, Osabutey et al. 2007; Dyson, Stidwill et al. 2007).

### 2.4.2 Cardiovascular response of mouse model of sepsis

Echocardiography is a useful tool to investigate cardiovascular function in animal models of sepsis (Ullrich, Scherrer-Crosbie et al. 2000; Hollenberg, Dumasius et al. 2001; Merx, Liehn et al. 2005). Simultaneous echocardiography and pressure measurements allow detailed study of the cardiovascular response to sepsis, and can be used to prognosticate.

Profound cardiovascular changes were seen within hours of induction of sepsis. In severely ill animals, aortic blood flow peak velocity (a marker of contractility) was almost halved at 6h and remained low at 24h. Stroke volume and cardiac output data followed this pattern. Heart rate failed to increase, perhaps related to the concurrent hypothermia. The LV cavity was visibly smaller at 6h (LV end-diastolic and end-systolic diameters were half baseline values) and hyperdynamic. At 24h LV cavity

sizes were also smaller but to a lesser extent, and the LV was clearly less dynamic in function. Fluid challenges at 6h resulted in significant haemodynamic improvements, whereas at 24h, after initial improvement, caused deterioration presumably due to volume overload. This suggests that hypovolaemia is the predominant early cause of a low cardiac output, while reduced myocardial contractility is responsible later on.

Septic myocardial dysfunction is characterized by reduced contractility, poor fluid responsiveness, and ventricular dilatation (Hollenberg, Dumasius et al. 2001; Zanotti-Cavazzoni, Guglielmi et al. 2009). I found all of these changes in this mouse model of sepsis at 24h. However, in a fluid resuscitated and antibiotic treated CLP mouse model, sepsis was associated with increasing cardiac output and heart rate (Hollenberg, Dumasius et al. 2001). These mice received 50ml/kg fluid boluses every 6 h. But crucially, in this study the measured stroke volumes were 50% lower than those obtained in my study. This difference in stroke volume was likely related to the anaesthetic technique used. There is a large inter-individual variation in the minimum alveolar concentration (MAC) of inhalational anaesthetics (Sear 1992), particularly with concurrent hypothermia and sepsis (Gill, Martin et al. 1995; Allaouchiche, Duflo et al. 2001). I used the minimum concentration of isoflurane needed to maintain anaesthesia with loss of the withdrawal reflex to pinch as the endpoint for each mouse at different time-points. This fluctuated from 1.5-2% isoflurane in non-septic mice to only 0.5% in the severely septic animals. By contrast, Hollenberg *et al* (Hollenberg, Dumasius et al. 2001) used a large single dose of intramuscular

ketamine/acepromazine that provides rapid onset deep anaesthesia, but redistribution and excretion of the drugs results in a variable depth of anaesthesia. The cardiac depression and low stroke volume they recorded may be, at least in part, related to this anaesthetic regimen.

The same group addressed this short-coming by using minimal concentrations of isoflurane during echocardiography (Zanotti-Cavazzoni, Guglielmi et al. 2009). In this latter study the effect on outcome from CLP-induced sepsis of three different fluid regimens (low, intermediate and high volume) were compared. Their stroke volume and cardiac output changes were very similar to values I obtained, but baseline heart rate and the percentage fall at 24h was lower. They also found that stroke volume incrementally increased with increasing fluid resuscitation. A high volume s/c fluid resuscitation regimen (335 ml/kg over first 24 h) also improved 24h survival. This is however equivalent to 23.5 litres given to a 70 kg patient over 24h, and nearly three-fold higher than the 130 ml/kg/day I administered. This fluid was given subcutaneously and in my model of sepsis, was incompletely absorbed as some of this fluid persisted and could be seen at post-mortem.

The pathophysiology of myocardial dysfunction in sepsis is multi-factorial (Rudiger and Singer 2007). In my model, the hypothermia that occurred concurrently in the severely septic mice also had a significant impact on cardiovascular parameters. Apart from profound effects on heart rate, hypothermia is also thought to affect myocardial contractility and cardiac afterload (Greene, Cameron et al. 1989; Polderman 2009). This was apparent in the severely septic mice as cardiac output doubled

upon re-warming to 37°C due to significant increases in both heart rate and stroke volume.

## 2.5 Conclusion

I developed and characterized a long-term, fluid-resuscitated murine model of sepsis that I felt to be suitable for the further studies performed in this body of work. The model manifests biochemical evidence of organ dysfunction with a mixed metabolic and respiratory acidosis, the degree of which is related to both clinical severity and the fall in core temperature. Oxygen consumption is reduced in line with both clinical severity and the fall in body temperature. However, this does not improve on rewarming despite a two-fold increase in cardiac output, and is suggestive of a direct effect of systemic inflammation on decreasing cellular metabolism and/or energy supply. Despite fluid resuscitation, the fall in cardiac output during the initial phase of sepsis appears to be predominantly due to hypovolaemia, however, by 24h, myocardial depression and an autonomic response appears more important.

Despite a similar infectious insult in mice of similar genotype, age, gender, food type and upbringing (often from the same litter), the septic phenotype varied markedly between animals. This indicates an important individual variation related to either transcriptional or post-transcriptional factors, and/or environmental influences such as previous exposure to infection. Mortality was related to the degree of clinical severity and could be prognosticated at an early stage in their septic process.

Although the septic phenotype does differ in some respects from that seen in the majority of septic patients, in particular the profound fall in temperature and oxygen consumption, many features are still shared.